BIOCHEMISTRY

Its own architect: Flipping cardiolipin synthase

Katsuhiro Sawasato, William Dowhan, Mikhail Bogdanov*

Current dogma assumes that lipid asymmetry in biological membranes is actively maintained and dispensable for cell viability. The inner (cytoplasmic) membrane (IM) of *Escherichia coli* is asymmetric. However, the molecular mechanism that maintains this uneven distribution is unknown. We engineered a conditionally lethal phosphatidylethanolamine (PE)–deficient mutant in which the presence of cardiolipin (CL) on the periplasmic leaflet of the IM is essential for viability, revealing a mechanism that provides CL on the desired leaflet of the IM. CL synthase (ClsA) flips its catalytic cytoplasmic domain upon depletion of PE to supply nonbilayer-prone CL in the periplasmic leaflet of the IM for cell viability. In the presence of a physiological amount of PE, osmotic down-shock induces a topological inversion of ClsA, establishing the biological relevance of membrane protein reorientations in wild-type cells. These findings support a flippase-less mechanism for maintaining membrane lipid asymmetry in biogenic membranes by self-organization of a lipid-synthesizing enzyme.

INTRODUCTION

Most, if not all, biological membranes display an asymmetric distribution of lipid species on each side of the lipid bilayer (*1*). Although eukaryotic cell plasma membrane lipid asymmetry is well established and loss and gain of asymmetry is associated with an array of cellular malfunctions (*2*), the physiological significance and detailed molecular mechanism by which membrane phospholipid asymmetry is generated, maintained, and controlled and its specific function in bacterial membrane–related processes are not clear (*1*, *3*). Diderm Gram-negative bacteria have two membranes: inner membrane (IM) and outer membrane (OM). Because most phospholipid molecules are synthesized on the cytoplasmic leaflet of the IM, newly synthesized lipids must be first translocated across the IM and then transported to the OM to build the cell envelope during bacterial growth (*3*). We recently reported vectoral chemical probes with different membrane-penetrating and chemical properties, and determined the head group and acyl-chain asymmetry of aminophospholipids using radiometric, mass spectrometric, and spectrophotometric approaches (*4*). Using this methodology, we demonstrated that the IM of *Escherichia coli* and *Yersinia pseudotuberculosis* is asymmetric with a 75%/25% (cytoplasmic/periplasmic leaflet) distribution of phosphatidylethanolamine (PE) in rod-shaped cells and an opposite distribution in filamentous cells (*4*). Although topography of anionic phospholipids phosphatidylglycerol (PG) and cardiolipin (CL) in the cytoplasmic membrane of these Gram-negative bacteria is still unknown, from experimentally determined transmembrane distribution of PE and total amounts of PG and CL in the IM, we predicted that the periplasmic leaflet of the IM contains more negatively charged phospholipids than the cytoplasmic leaflet (*4*).

CL is a chemically and structurally unique lipid because, unlike other canonical phospholipids, it has four hydrophobic acyl chains and two negative charges attributed to phosphodiester bonds. *E. coli* has three distinct enzymes synthesizing CL: ClsA, ClsB, and ClsC (*5*–*7*). Although none of the three gene products are essential for viability under laboratory conditions (*5*, *8*), CL-deficient cells show pleiotropic effects such as defects in the assembly of the polytopic membrane protein LacY, membrane bilayer translocation of periplasmic protein PhoA, and protein folding and assembly of the OM protein OmpF (*9*–*11*). Moreover, CL-deficient strains display activation of Rcs envelope stress response, alter envelope ultrastructure, and exhibit less efficient transport of underacylated KDO_2–Lipid A substrate by MsbA (*10*–*12*). All these CL-dependent events would limit bacterial cell survival, cell fitness, or ability to adapt to stressed conditions. CL is involved in maintaining cell size and proper cell division (*13*, *14*). CL occupies different IM leaflet distributions at the cell poles and septa of *E. coli* as determined by the CL-specific probe Erylysin A (EryA)–enhanced green fluorescence protein (EGFP) chimeric protein (*15*). The binding of EryA-EGFP to CL on the periplasmic leaflet of the IM interferes with cell division resulting in chain morphology (*15*), suggesting that CL dynamically redistributes along the IM during the cell division. Theoretically, the large hydrophobic domain and charge of dianionic CL may require a flippase for it to undergo transbilayer movement like that of bulky tetra-acyl KDO_2–Lipid A (lipopolysaccharide), which requires the adenosine triphosphate–dependent MsbA lipid translocase (floppase) (*16*). However, thus far, only one flippase for glycerophospholipids has been identified in Gram-negative bacteria, which synthesizes and translocates noncanonical cationic *O*-lysyl-PG across the IM of plant pathogens (*17*, *18*). Although a prior localization and/or different orientations of catalytic sites of individual CL biosynthetic enzymes could account for IM leaflet-specific CL insertion into the bilayer (*2*), the membrane topology of the primary ClsA has been controversial for the past 30 years (*19*, *20*). Thus, why and how CL is distributed on both sides of the IM are still unknown.

All biological membranes contain a spectrum of lipid species with diverse molecular shapes and differing in the number of acyl chains, chain length, unsaturation, and head group composition. A delicate balance between these molecular shapes and phase properties is necessary for a functional membrane (*21*). A balance is maintained between the lamellar phase preferring lipids and those that adopt a nonbilayer organization while providing large chemical diversity. As a result, a diversity of physical and chemical properties is available to support the structure and function of the many membrane-associated proteins. PE if unsaturated or CL in the presence of divalent cations (Mg^{2+}, Sr^{2+}, or Ca^{2+} but not Ba^{2+}) has a strong propensity to adopt inverted nonbilayer structures (*22*, *23*). Knockout studies of the three CL synthase (*clsA*, *clsB*, and *clsC*) and the phosphatidylserine synthase (*pssA*) genes, which encode the enzymes that synthesize CL and

Department of Biochemistry and Molecular Biology, McGovern Medical School, The University of Texas Health Science Center at Houston, Houston, TX 77030, USA.
*Corresponding author. Email: mikhail.v.bogdanov@uth.tmc.edu

the committed step to PE biosynthesis, respectively, have shown that, individually, neither CL nor PE is essential for the viability of *E. coli* under defined laboratory conditions (*5*, *8*, *23*). At the same time, PE-lacking cells are viable but have an absolute requirement for both the *clsA* gene product and divalent cations (Mg^{2+}, Sr^{2+}, or Ca^{2+} but not Ba^{2+}) presumably because CL per se is unable to make sufficient type II (inverted cone-shaped) structures without specific divalent cations (*22*). Because Ca^{2+} is actively pumped out of the cytoplasm and maintained intracellularly at micromolar levels (*24*), and concentrations of Mg^{2+} in the cytoplasm are maintained in a range of 50 to 100 mM independent of the concentration of Mg^{2+} in the growth medium (*25*), we proposed that the requirement of higher concentrations of divalent cations must be on either the periplasmic leaflet of the IM or OM (*22*, *23*). Thus, an adequate amount of CL, in the presence of the specific divalent cations, must be delivered to the periplasmic leaflet of the IM or OM to support the growth of PE-deficient cells to substitute for the nonbilayer phase-forming ability of PE. In our recent study, the experiments with leaflet-specific lipid packing order–sensitive fluorescent probe NR12S and leaflet nonspecific push-pull pyrene analog (PA) demonstrated that lipid packing order only on the periplasmic leaflet of the IM was progressively decreased as the PE level was decreased (*4*). Because disruption of CL biosynthesis increased lipid order in the IM, CL contributes to decreased lipid order in the periplasmic leaflet of the IM in response to reduced PE levels. These observations suggest the existence of a putative mechanism, which is operating to increase the amount of CL in the periplasmic leaflet of the IM to satisfy the requirement of nonbilayer forming lipid in the periplasmic leaflet of the IM in response to a decreased amount of PE. Therefore, a strain in which the amount of PE and CL can be finely tuned could be a powerful genetic tool to discover a mechanism by which CL is delivered to the periplasmic leaflet of the IM.

The lack of both PE and CL cannot be suppressed to allow growth under any condition thus far tested, and the requirement for Mg^{2+} in the absence of PE is a very strong growth phenotype. Although we have never been able to bypass the divalent metal ion requirement in a PE-lacking strain, a conditionally lethal mutant was engineered in which the amount of PE can be controlled and each *cls* gene was expressed one at the time either from the chromosome or a plasmid. These engineered conditionally lethal mutant strains and their Mg^{2+} auxotrophy allowed us to address the physiological significance of *cls* gene multiplicity, understand why PE-lacking cells are Mg^{2+} auxotrophs, and determine whether CL and a divalent cation requirement are interior or exterior to the IM.

Although the membrane topology of ClsA has been controversial (*19*, *20*), we found that ClsA adopts a uniform topology with the catalytic domain facing cytoplasm in wild-type cells. Unexpectedly, we found that ClsA flips its catalytic globular domain upon depletion of PE to supply CL in the periplasmic leaflet of the IM. The truncation of N-terminal transmembrane regions of ClsA diminished the flippability of ClsA with an accumulation of CL in the cytoplasmic leaflet of the IM. Thus, the primary CL synthase ClsA retains or flips its catalytic domain providing CL on the desired leaflet of the IM to satisfy the requirement for nonbilayer-prone CL to support the growth of PE-deficient cells. These discoveries demonstrate the self-organization potential of lipid biosynthetic enzymes in Gram-negative bacteria. Furthermore, we demonstrated that an osmotic down-shock induces inversion of ClsA even in the presence of a physiological amount of PE. Because the expansion of the cell volume is accompanied by an increase in the elastic tension of the IM due to stretching of the cell envelope upon osmotic down-shock, we propose that both PE and IM in-plane tension set a threshold level for flippability of ClsA, which is structurally unrelated to a subset of thus far identified flip-flopping membrane proteins. These membrane proteins can switch their orientation in the membrane in response to changes in membrane lipid composition or cell physiology, contrary to long-standing dogma in membrane biology (*26*). The dual membrane orientation of ClsA demonstrates the physiological significance of the membrane protein flip-flopping phenomenon in Gram-negative bacteria.

RESULTS

Primary CL synthase (ClsA) is essential and sufficient to support Mg-dependent growth of PE-deficient cells

E. coli has three genes that encode CL synthases; however, the significance of this multiplicity is still unclear. Most prokaryotes express multiple CL synthases with ClsA being the primary activity in *E. coli*. There is little understanding of the function of the other two enzymes in this and other bacteria (*27*–*29*). ClsA is present under all growth conditions, whereas ClsB and ClsC are induced during late log and stationary phases (*5*). It is assumed that ClsA is essential for the growth of PE-deficient cells because a plasmid temperature-sensitive for replication encoding the *pssA* gene cannot be cured from PE-deficient cells containing a null allele of the *clsA* gene (*23*). Also, a null allele of the *clsA* gene cannot be introduced into a Δ*pssA* strain via P1 transduction (*23*). Despite these experimental facts, the role that each Cls plays in the viability of PE-deficient cells has not been investigated. To decipher which *cls* gene is responsible for the divalent cation-dependent growth of PE-deficient cells, we engineered strain KS310 (Δ*pssA93*::*kan* $P_{LtetO-1}$-*pssA*) carrying null alleles of the *cls* genes on the chromosome (listed in table S1). In these strains, the chromosomal *pssA* gene is disrupted by insertion of the kanamycin-resistant gene (*kan*), and a wild-type *pssA* gene allele is integrated at the *attB* site on the chromosome and under the control of *tet* promoter ($P_{LtetO-1}$ promoter), allowing regulation of PE levels by variable amounts of anhydrotetracycline (aTc) in the growth medium (Fig. 1A). We also introduced individual plasmid-borne copies of each of the *cls* genes under the control of the arabinose-inducible promoter (P_{araBAD}) into KS410 (strain KS310 Δ*clsABC*). Therefore, each *cls* gene could be individually expressed under either a plasmid independent of normal cellular control or the chromosome under cellular control. The strong promoter $P_{LtetO-1}$ integrated into the *attB* site on chromosome allows the regulation of the *pssA* gene expression over a 5000-fold range with aTc as an inducer. Isopropyl-β-D-1-thiogalactopyranoside (IPTG) and arabinose regulation of *cls* gene expression by $P_{lac/ara-1}$ is controllable over a 1000-fold range (*30*).

We tested the ability of each Cls to support growth as a function of PE levels (2 to 75%) titrated by inducer aTc and CL levels titrated by inducer arabinose or the expression of *cls* genes from the chromosome. We took advantage of the observation that a $pssA^{ts}$ Δ*clsA* strain, which accumulated only 20 to 30% of PE, was viable at the restrictive temperature in a medium containing 50 mM $MgCl_2$ plus 400 mM sucrose (*31*). Osmotic stabilization of cell envelopes by sucrose appears to allow the growth of a strain compromised in PE synthesis when the CL level is very low (*31*). The results of plating each of these strains in the presence or absence of aTc on agar plates containing 50 mM $MgCl_2$ with or without 400 mM sucrose are shown in Fig. 1 (B and D). The amount of PE in KS310 grown with

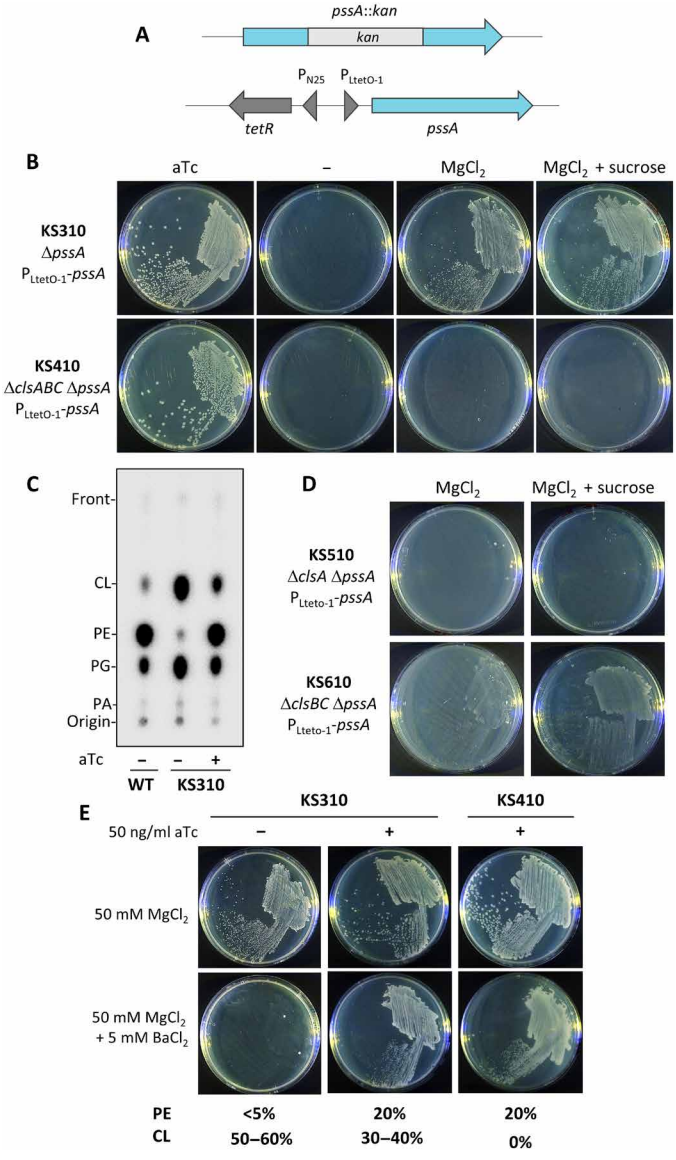

Fig. 1. Deciphering the role of *cls* gene multiplicity in Mg-dependent growth of PE-deficient cells. (**A**) Schematic representation of the genetic organization of the Δ*pssA*/$P_{LtetO-1}$-*pssA* mutant. (**B**) Growth phenotype of -PE and -PE/-CL mutants. Indicated strains were streaked on LB agar medium with supplementation of aTc (100 ng/ml) and 50 mM $MgCl_2$ with or without 400 mM sucrose as indicated above each plate. These cells were incubated for 24 hours at 37°C. (**C**) TLC analysis of the phospholipid composition of wild type (WT; W3110) and KS310. An overnight culture of KS310 grown with aTc (200 ng/ml) was washed three times with fresh LB medium. Then, cells were diluted into fresh LB medium containing 50 mM $MgCl_2$ with or without aTc (500 ng/ml) and grown to OD_{600} 0.05. Wild-type cells were diluted into fresh LB medium to OD_{600} 0.05. Cells were grown to the mid-log phase (OD_{600} 0.6 to 0.8) with [^{32}P]PO_4 (1 μCi/ml), and phospholipids were extracted as described in the Materials and Methods. Individual phospholipids were separated by TLC using solvent 2 and then visualized using Phosphoimager. (**D**) Role of individual *cls* genes in the Mg-dependent growth of PE-deficient cells. Indicated strains were streaked on LB agar medium containing 50 mM $MgCl_2$ with or without 400 mM sucrose. (**E**) Effect of Ba^{2+} on the Mg-dependent growth of the cells with different threshold amounts of PE. Indicated strains were streaked on LB agar medium containing 50 mM $MgCl_2$ with or without 5 mM $BaCl_2$. The mol % of PE and CL in these strains in liquid culture is noted under each plate.

50 mM $MgCl_2$ in the absence of aTc was <5%, and the PE level can be restored to the wild-type level by supplementation of aTc (Fig. 1C and fig. S2A). As expected, the lethal phenotype of KS310 (low PE plus CL) but not KS410 (low PE and no CL) in the absence of aTc was suppressed by the presence of 50 mM $MgCl_2$ (Fig. 1B). The addition of 400 mM sucrose into the growth medium did not support the growth of KS410 even in the presence of 50 mM $MgCl_2$ (Fig. 1B), indicating that CL is required to support the Mg-dependent growth of PE-deficient cells. The disruption of the *clsA* gene of KS310 (strain KS510: Δ*clsA* Δ*pssA*/$P_{LtetO-1}$-*pssA*) resulted in the loss of viability in the presence of 50 mM $MgCl_2$ (Fig. 1D), indicating that ClsA is essential for Mg-dependent growth of PE-deficient cells. On the other hand, the disruption of both the *clsB* and *clsC* genes of KS310 resulting in the new strain KS610 (Δ*clsB* Δ*clsC* Δ*pssA*/$P_{LtetO-1}$-*pssA*) allowed the growth in the presence of either 50 mM $MgCl_2$ or 50 mM $MgCl_2$ + 400 mM sucrose media (Fig. 1D). ClsA either being chromosomal (Fig. 1D) or expressed from a plasmid (fig. S1) supports growth under both conditions. The overexpression of neither ClsB nor ClsC supported Mg-dependent growth of KS410 (fig. S1). These results indicate that ClsA is sufficient to phenocopy the KS310 strain and support the divalent cation growth requirement of PE-deficient cells under the conditions we examined.

The threshold level of PE determines the requirement of CL for the Mg-dependent growth of cells with low PE levels

As mentioned above, in the presence of an intermediate amount of PE (20%), ClsA is not essential. However, supplementation with both 50 mM $MgCl_2$ and 400 mM sucrose is still required for the growth of the $pssA^{ts}$ Δ*clsA* mutant at nonpermissive temperature (*31*), suggesting that this amount of PE is sufficient to satisfy the nonbilayer phase growth requirements on the periplasmic leaflets of the IM and OM. If this is the case, then Mg-dependent growth of these cells should not be inhibited by Ba^{2+}, which arrests the growth of PE-deficient cells due to the interference of Ba^{2+} cations with the nonbilayer behavior of the CL (*22*). To what extent can CL in combination with different divalent cations replace PE in the membrane of *E. coli* cells and vice versa? A chromosomal copy of $P_{LtetO-1}$ controlling expression of the *pssA* gene can be regulated uniformly throughout the cell culture from near-zero to wild-type level (75 to 80%) proportional to the amount of gene inducer aTc in the growth medium (fig. S2B). Therefore, to verify our hypothesis, we tested whether the Mg-dependent growth of KS310 cells synthesizing around 20% of PE is inhibited by Ba^{2+}. We confirmed the presence of around 20% of PE when outgrown in the media supplemented with aTc (50 ng/ml) plus 50 mM $MgCl_2$ (fig. S2B). The Mg-dependent growth of KS310 outgrown without aTc (<5 mol % of PE) was inhibited by adding 5 mM $BaCl_2$ into the growth medium (Fig. 1E). On the other hand, the growth inhibition effect of Ba^{2+} was not observed in the presence of aTc (50 ng/ml) (Fig. 1E). These observations indicate that the growth requirements of a nonbilayer-prone lipid are fully satisfied by PE independent of nonbilayer phase property of CL on the periplasmic leaflet of either the IM or OM when only 20% of PE is synthesized. Consistent with this notion, KS410 was able to grow when aTc (50 ng/ml) was present, and Mg^{2+}-supported growth of KS410 was insensitive to the addition of 5 mM $BaCl_2$ to the growth medium (Fig. 1E), indicating that all *clsABC* genes are not essential for growth when 20% of PE is present. The same results were observed when we used conditionally lethal

UE81 (Δ*pssA*::*cat* P_{araBAD}-*pssA*) in which the chromosomal *pssA* gene is replaced by the chloramphenicol-resistance gene (*cat*) and a wild-type *pssA* allele is expressed from an arabinose promoter (*32*). The growth of UE81 is dependent on the addition of arabinose to the growth medium, and the lethal phenotype in the absence of arabinose was suppressed by the addition of Mg^{2+} to the growth medium (fig. S2D). This strain accumulates 20% of PE without an inducer due to the basal expression from the arabinose promoter (fig. S2C). The growth of UE81 in the presence of 50 mM $MgCl_2$ was not inhibited by adding 5 mM $BaCl_2$ into the growth medium (fig. S2D). Also, all *clsABC* genes were not necessary to support the Mg-dependent growth of UE91 (Δ*clsABC* Δ*pssA* P_{araBAD}-*pssA*), and the Mg^{2+}-supported growth of UE91 was insensitive to the addition of 5 mM $BaCl_2$ to the growth medium (fig. S2D). Therefore, the requirement of nonbilayer-prone CL for growth can be observed only when the amount of PE is less than 20%.

ClsA adopts a dual topology in PE-deficient cells

ClsA is predicted to be composed of two N-terminal transmembrane domains (TMDs) including residues 3 to 23 and 38 to 58 followed by a soluble globular phospholipase D phosphodiesterase catalytic domain containing two conserved HKD motifs (HxKxxxxD) (Figs. 2A and 3A and fig. S4). Based solely on structural bioinformatics, ClsB and ClsC contain no predicted TMD helices (fig. S3). However, both activities were found in the IM fraction (*5*, *6*), suggesting that they are membrane-associated proteins. There is current controversy surrounding the catalytic site orientation of ClsA, which resides in a large C-terminal globular extramembrane domain (EMD) containing five cysteine residues. Two different transmembrane topologies of ClsA have been proposed, exposing the catalytic globular domain on either side of the IM (Fig. 2A) (*33*). We assumed that, if the globular domain of ClsA is on the periplasmic side of the IM, CL can be directly synthesized and supplied in the periplasmic leaflet of the IM.

ClsA-catalyzed reactions are reversible in vivo and in vitro and use other sugar alcohols in place of glycerol to reverse CL synthesis. Original evidence for a periplasmic orientation of the ClsA active site came from experiments showing that feeding *E. coli* cells 600 mM mannitol results in the formation of phosphatidylmannitol (PM) and diphosphatidylmannitol (DPM) in a ClsA-dependent manner (*19*). Mannitol is taken up by the MtlA transport system and is immediately converted in a coupled reaction to mannitol-P, which should not be a substrate in the reverse reaction. Disruption of the MtlA did not affect the synthesis of these glycolipids (*19*). The authors concluded that the active site of ClsA (ClsBC were unknown at the time) faces the periplasm. However, recent topological mapping of native cysteines with membrane-impermeable fluorophore Oregon Green maleimide and subsequent analysis of immunoprecipitated ClsA-His_{10} suggested that the catalytic domain faces the cytoplasm in wild-type cells (*20*). However, the C-terminally tagged ClsA-His_{10} (*20*) or ClsA-His_6 (*34*) are inactive both in vivo and in vitro. According to the positive-inside rule (*35*, *36*), the hydrophilic interhelix loop connecting the two TMDs and the hydrophilic domain connecting the second TMD to the globular domain containing multiple positive charges (Fig. 3A) should tend to reside in the cytoplasm, thus allowing the C-terminal globular domain to face the cytoplasm (designated as $ClsA_{cyto}$ in Fig. 2A) (*33*). Moreover, the conserved proline and glycine (PxxG) residues (Fig. 2A and fig. S4) can "melt" the middle of the second TMD and force this domain to adopt a membrane-dipping conformation (*33*) often referenced as a reentrant loop starting and ending on the same side of membrane (Fig. 2A). Accordingly, AlphaFold2 predicts that the second TMD of ClsA adopts a U-shaped mini-loop conformation (fig. S5) (*37*). We assumed that the amount of PE can explain the discrepancy in the predicted membrane topologies of ClsA proposed independently by two labs. Shibuya's lab (*19*) reported that the formation of PM and DPM drastically increased when the PE level was reduced in the temperature-sensitive *pss-1* mutant outgrown at a nonpermissive temperature. We previously demonstrated that a subset of membrane proteins undergoes topological inversion when PE levels decline (*38*–*44*). These observations suggest that dropping the PE level could potentially affect the topology of ClsA.

Thus, we decided to reinvestigate the orientation of the globular catalytic domain of ClsA. Because C-terminally tagged ClsA's are not active, we engineered an internal EYMPME (EE) epitope tag within the globular catalytic domain beginning at amino acid residue 296 of ClsA. Because ClsA has three of the six amino acids that comprise the EE tag, we introduced three mutations, N295E, I297Y, and F300M, into ClsA. However, we found that the F300M substitution was sufficient to detect the protein by immunoblotting analysis with anti-EE tag antibodies. We decided to use ClsA F300M as an EE-tagged ClsA [ClsA (EE)] to minimize the effect of mutation on enzymatic activity and membrane topology. Expression of plasmid-borne ClsA (EE) and wild-type ClsA in CL-deficient cells (BKT12: Δ*clsABC*) cells resulted in biosynthesis of essentially the same amount of CL (fig. S6A). Plasmid-borne ClsA (EE) supported Mg-dependent growth of conditionally lethal KS410 (fig. S6B). These results indicate that ClsA (EE) is fully active as a membrane-associated enzyme. The open reading frame of the *clsA* gene predicts a 54.8-kDa polypeptide. In all previous reports, partially purified (*45*, *46*), radiolabeled plasmid-borne (*7*), and C-terminal His-tagged inactive ClsA (*20*) migrated with an apparent molecular weight of 46 to 48 kDa on SDS–polyacrylamide gel electrophoresis (PAGE), suggesting that posttranslational processing occurs. When a total membrane fraction prepared from BKT12 expressing ClsA (EE) was subjected to SDS-PAGE/immunoblotting analysis, we observed that arabinose-induced epitope-tagged membrane-associated ClsA migrates with an apparent molecular mass of 46 kDa (fig. S7A). However, we also observed that several nonspecific bands migrated close to ClsA (EE) (indicated as #, ##, and ### in fig. S7A). To eliminate the presence of these nonspecific bands, we performed the membrane differential fractionation by a two-step ultracentrifugation. In this analysis, a heavier membrane fraction was removed by an initial centrifugation at 88,000*g*. The remaining membrane was collected by centrifugation at 200,000*g*. We found that most of the ClsA (EE) was collected in the membrane fraction during the first centrifugation (fig. S7B). Fortunately, the nonspecific bands situated close to ClsA (EE) (fig. S7A) were predominantly found in membrane fractions obtained after the second centrifugation (fig. S7B). Thus, we used membrane fraction obtained after the first step of lower-speed ultracentrifugation for further analysis unless specified. Even if the residual nonspecific bands were present in the membrane fraction after the first ultracentrifugation step, these bands could be separated by running the SDS-PAGE longer (fig. S7C). We also observed that ClsA runs at a lower apparent molecular weight (EE)* after treatment at 100°C than at its predicted molecular weight (EE) after treatment at 37°C, as shown in Fig. 2B. This anomalous gel behavior and mobility of ClsA (EE) might be due to incomplete denaturation by SDS, which result in the retaining of a high degree of secondary

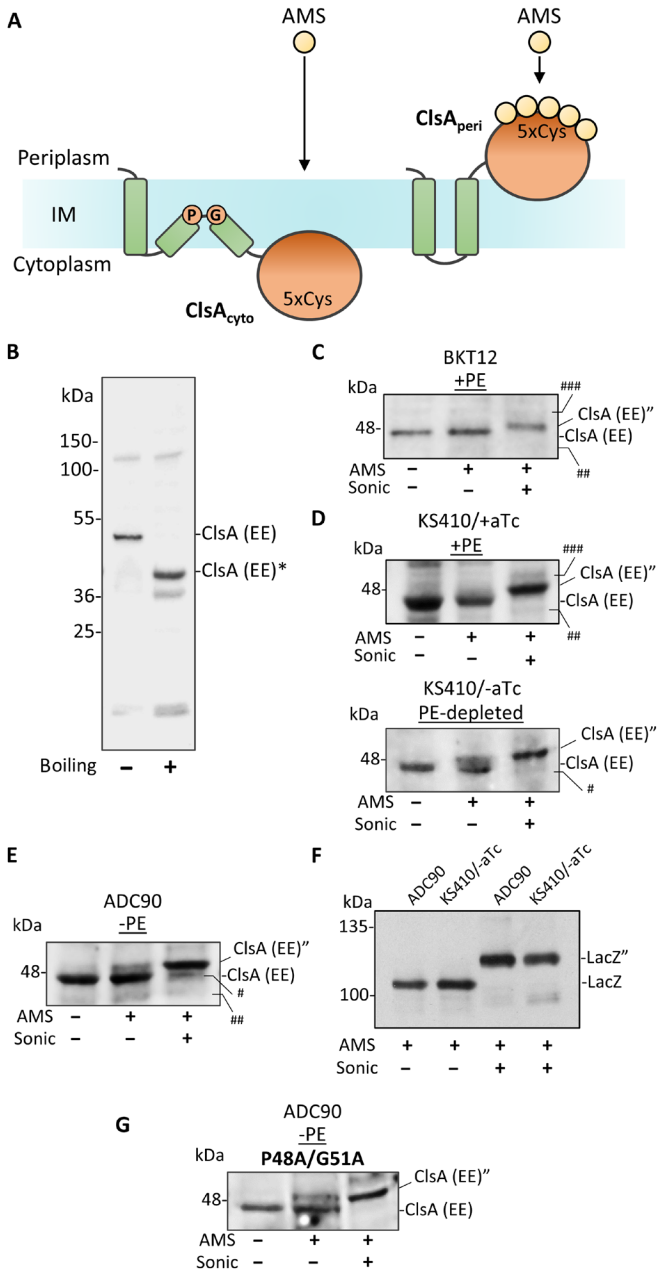

Fig. 2. Mapping the membrane topology of ClsA conformers. (**A**) Schematic representation of the putative membrane topology of ClsA. (**B**) Detection of ClsA (EE) by SDS-PAGE/immunoblotting. BKT12 harboring pBAD30-ClsA (EE) were grown with 0.2% arabinose to OD_{600} 0.6 to 0.8. A total membrane fraction was prepared as described in the Materials and Methods. The membrane fraction dissolved in the SDS-PAGE sample buffer was incubated at 37°C (–) or 100°C (+) for 10 min before loading 10 μg of the total membrane protein to the acrylamide gel. ClsA (EE) was detected by using an anti–EE tag antibody after electroblotting. (**C**) Membrane topology of ClsA (EE) in +PE cells. BKT12 harboring pBAD30-ClsA (EE) were grown in LB medium containing 0.02% arabinose. When the cell density reached OD_{600} 0.6 to 0.8, the membrane topology of ClsA (EE) was assessed by ECAM. An AMS-derivatized ClsA (EE) is indicated as ClsA (EE)". (**D**) Membrane topology of ClsA (EE) in PE-depleted cells. An overnight culture of KS410 harboring pBAD30-ClsA (EE) grown with aTc (200 ng/ml) was washed three times with fresh LB medium. After that, cells were diluted into fresh LB medium containing 50 mM $MgCl_2$ with (+PE) or without (PE-depleted) aTc (500 ng/ml). After growing the cells until the mid-log phase (OD_{600} 0.6 to 0.8), the membrane topology of ClsA (EE) was assessed by ECAM. Expression of ClsA (EE) was induced by adding 0.02% arabinose into the growth medium. (**E**) Membrane topology of ClsA (EE) in PE-deficient (-PE) cells. ADC90 harboring pTac-ClsA (EE) was grown in LB medium containing 50 mM $MgCl_2$. The growth medium was made 10 μM in IPTG to induce expression of ClsA (EE). Membrane topology of ClsA (EE) was determined by ECAM. (**F**) Assessment of the intrinsic IM impermeability to AMS of PE-deficient cells expressing ClsA (EE). PE-deficient cells derived from two different host backgrounds were used. PE in KS410 harboring pBAD30-ClsA (EE) was depleted as described in (C). ADC90 harboring pTac-ClsA (EE) was grown as described in (D). Intact or disintegrated cells were incubated with 1 mM AMS for 60 min at 25°C, imitating the conditions for ClsA ECAM experiments. Intact cells were disintegrated by ultrasonication, and the cytoplasmic fractions were retained after removal of the membrane fraction by ultracentrifugation (200,000*g*) for subsequent SDS-PAGE and Western blotting with anti-LacZ monoclonal antibodies. (**G**) Role of the PxxG motif in the membrane topology of ClsA (EE). Membrane topology of ClsA (EE) P48A/G51A in PE-deficient (-PE) cells [ADC90/pTac-ClsA (EE)] was assessed. The growth medium was made 10 μM in IPTG to induce expression of ClsA (EE) P48A/G51A.

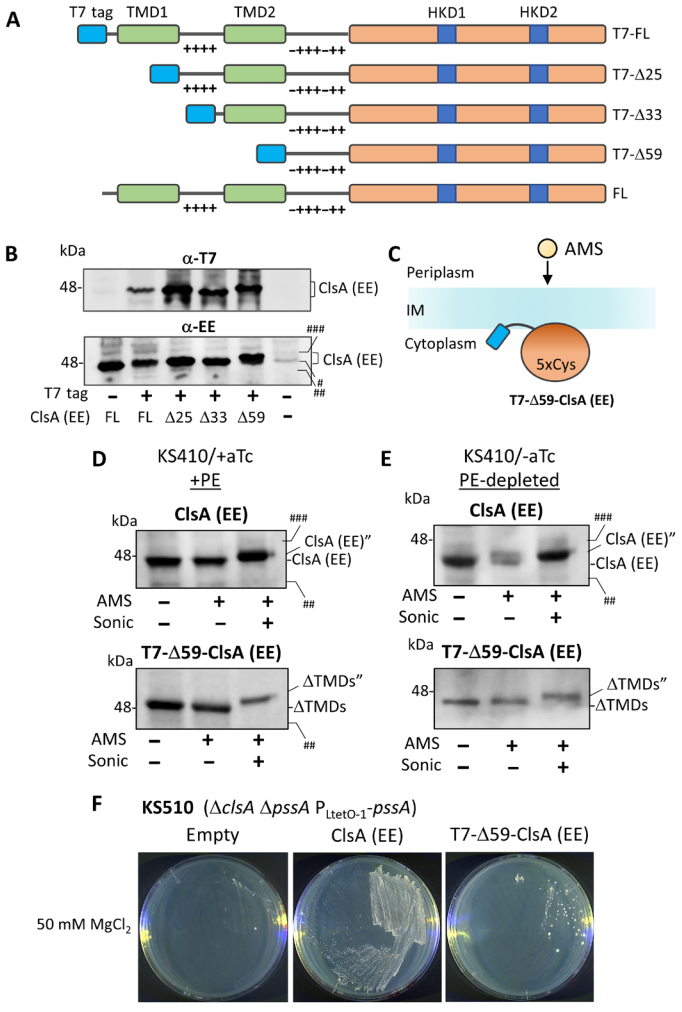

Fig. 3. Role of N-terminal TMDs of ClsA in the generation of an inverted topology and divalent cation-dependent growth of PE-deficient cells. (**A**) Schematic representation of incrementally truncated ClsA (EE) with T7 tag at its N terminus. Two TMDs and the hydrophilic extramembrane region of ClsA are shown as green boxes and black lines, respectively. The C-terminal globular domain of ClsA is shown as an orange box with blue boxes corresponding to the HKD motif of ClsA. (**B**) Detection of ClsA derivatives by SDS-PAGE/immunoblotting. BKT12 expressing ClsA (EE) or its derivatives from a pBAD18 plasmid were grown with 0.02% arabinose. When the cell density reached OD_{600} 0.6 to 0.8, cells were collected, and then the total membrane fraction was prepared. Ten micrograms of the protein were subjected to SDS-PAGE/immunoblotting. ClsA (EE) was detected either by an anti–T7 tag antibody (upper panel) or by an anti–EE tag antibody (lower panel). # indicates a nonspecific band. (**C** to **E**) Membrane topology of ClsA (EE) and TMD-less ClsA (EE) in +PE and PE-depleted cells. KS410 harboring pBAD18-ClsA (EE) or pBAD18-T7-Δ59-ClsA (EE) was grown as described in Fig. 2C, followed by an assessment of the membrane topology of ClsA (EE) by ECAM. KS410 grown with aTc (50 ng/ml) (D) and without aTc (E) were used for +PE and PE-depleted cells, respectively. (**F**) Growth complementation assay of conditionally lethal -PE/-CL cells. KS510 harboring either pBAD18-ClsA (EE) or pBAD18-T7-Δ59-ClsA (EE) was streaked on LB agar medium containing 50 mM $MgCl_2$. The agar plates were incubated for 24 hours.

structure and altered detergent binding (*47*). Both events are affected by temperature, and many membrane proteins display lower than predicted molecular size when treated at 100°C in SDS.

The orientation of the catalytic domain of ClsA relative to the membrane bilayer within the IM containing or lacking PE was determined by the gel shift–based endogenous cysteine accessibility method (ECAM). In this assay, the membrane-impermeable cysteine-specific reagent 4-acetoamido-4′-maleidylstibene-2,2′-disulfonic acid (AMS) was used to derivatize the endogenous native cysteine residues residing only in the globular domain of ClsA. AMS is widely used to determine the topology of membrane proteins because it has two charged sulfonate groups and is highly soluble in water. The size and the charged nature of this reagent result in its widely demonstrated inability to cross the cytoplasmic membrane of bacteria (*48*–*50*). Moreover, AMS adds 0.5 kDa to the target protein and therefore can be used as a mobility shift reagent. Because ClsA has five native cysteine residues in the C-terminal globular domain (Fig. 2A and fig. S5), the AMS derivatization of these cysteine residues of ClsA would result in a mobility upshift of about 2.5 kDa on SDS-PAGE. AMS treatment of ClsA (EE) in the presence of 1% SDS resulted in a mobility upshift of the protein in SDS-PAGE (fig. S7D). However, ClsA (EE) was not further upshifted even after the reducing reagent tris(2-carboxyethyl)phosphine hydrochloride (TCEP) was added (fig. S7E), indicating that all cysteine residues behave as free thiols and do not form intra- or intermolecular disulfide bonds. We confirmed that nonspecific bands situated close to ClsA (EE) were not derivatized by AMS irrespective of the presence or absence of TCEP (fig. S7F), indicating that contamination with these nonspecific bands does not affect the results of ECAM. If the globular domain is exposed to the periplasm (designated as $ClsA_{peri}$ topology), then externally added AMS to intact cells would derivatize cysteine residues of the globular domain (Fig. 2A, right), resulting in a shift in mobility of the protein on SDS-PAGE. If ClsA adopts a $ClsA_{cyto}$ topology, then membrane-impermeable AMS would not derivatize the globular domain of ClsA (Fig. 2A, left), and a mobility upshift would not be observed. Moreover, the reaction of native cysteines with nonpermeant AMS after cell disruption by sonication would be an independent indicator of the globular domain facing the cytoplasm.

First, we examined the membrane topology of the catalytic globular domain of ClsA (EE) in +PE cells. BKT12 cells harboring pBAD30-ClsA (EE) were outgrown with arabinose inducer until the optical density at 600 nm (OD_{600}) reached 0.6 to 0.8 followed by ECAM analysis. Although ClsA (EE) was not derivatized by externally added AMS, the disruption of the cell membrane by ultrasonication resulted in a mobility upshift of ClsA (EE) (Fig. 2C). To analyze the membrane topology of ClsA (EE) from the "lighter" membrane fraction characterized by relatively lower sedimentation velocity, this fraction was prepared by two-step ultracentrifugation after AMS labeling of intact cells. We observed that ClsA (EE) from the lighter membrane fraction was also not derivatized by externally added AMS performed prior to membrane fractionation (fig. S7G). These results indicate that all populations of ClsA (EE) uniformly adopt a $ClsA_{cyto}$ topology in +PE cells. To map the topology of ClsA in conditionally lethal mutant KS410 (Δ*clsABC* Δ*pssA*/$P_{LtetO-1}$-*pssA*) harboring pBAD30-ClsA (EE) under the +PE and PE-depleted conditions, this strain was outgrown with aTc overnight, and then PE was depleted from cells by washing out inducer aTc with the growth medium supplemented with 50 mM $MgCl_2$. The amount of PE in KS410 expressing ClsA (EE) grown under these conditions was less than 5% (fig. S8A). To maintain a physiological level of PE (fig. S2B), washed cells were grown with aTc (500 ng/ml) and 50 mM $MgCl_2$.The derivatization of ClsA (EE) by externally added AMS was not observed when cells were grown with aTc (Fig. 2D). In contrast to +PE cells, a fraction of ClsA (EE) was derivatized by externally added AMS in PE-depleted intact cells and the remaining ClsA (EE) was fully derivatized by AMS when membranes

were disrupted by sonication (Fig. 2D, lower panel). These results indicate that a substantial subpopulation of ClsA (EE) adopts a $ClsA_{peri}$ topology with the catalytic domain facing the periplasm in PE-depleted cells. Because PE cannot be completely depleted in KS410 (fig. S8A) and not all ClsA (EE) was derivatized under the conditions, AMS-inaccessible ClsA (EE) can correspond to a properly oriented population of ClsA synthesized before PE is depleted. To independently confirm that ClsA (EE) displays a dual topology in PE-deficient cells, we constructed strain ADC90 (Δ*pssA*::*kan* Δ*clsA*::*Tn10*) in which both *pssA* and *clsA* genes on the chromosome are disrupted. To support the Mg-dependent growth of this strain, ClsA (EE) was expressed from an IPTG-inducible promoter on a plasmid [pTac-ClsA (EE)]. After confirmation of the absence of PE in ADC90/pTac-ClsA (EE) (fig. S8B), the membrane topology of ClsA (EE) in ADC90 was assessed by ECAM. As shown in Fig. 2E, ClsA (EE) was not fully derivatized by externally added AMS. However, the remaining ClsA (EE) was derivatized when membranes were disrupted by sonication. To validate the intrinsic permeability of PE-deficient cells to AMS, we used β-galactosidase (LacZ) as a bona fide cytosolic bacterial marker. LacZ is an abundant cytoplasmic protein that is rich in surface-exposed cysteine residues and was used by us previously to test the intrinsic permeability of thiol-specific dimethyl sulfoxide–soluble MPB [3-(*N*-maleimidylpropionyl)biocytin] (*51*) and water-soluble MEOB [(+)-biotinyl-3-maleimidopropionomidyl-3,6-dioxaoctan ediamine] (*48*). Thus, an experiment with AMS was carried out under ECAM conditions except that the soluble fraction rather than the membrane fraction was analyzed. PE-deficient cells with different genetic backgrounds [ADC90/pTac-ClsA (EE) and KS410/pBAD30-ClsA (EE)] were outgrown with 0.5 mM IPTG for LacZ synthesis, followed by ECAM. A single protein band migrating near 118 kDa was observed in the cytoplasmic fraction of both PE-deficient cells with an expected molecular weight of the monomeric form of LacZ with a molecular mass of 116 kDa (Fig. 2F). Because AMS adds 0.5 kDa and LacZ does not contain disulfide bonds and all 16 cysteine residues are in the reduced form (*52*), AMS derivatization of these cysteine residues would result in a mobility upshift of about 8 kDa on SDS-PAGE. As observed in Fig. 2F, AMS derivatization of LacZ resulting in a mobility upshift was observed only when cells were disrupted by sonication before AMS treatment. Therefore, PE-deficient IMs are not permeable to AMS under our experimental conditions demonstrating the validity of using AMS-aided ECAM to map the topological organization of ClsA in PE-deficient cells. All these results indicate that ClsA displays a dual topology in PE-deficient cells and cells with a low threshold level of PE.

A conserved PxxG motif is not necessary for ClsA to adopt a dual topology

A PxxG motif in the middle of the second TMD of ClsA is evolutionarily conserved in ClsA in both Gram-negative and Gram-positive bacteria with minor exceptions (fig. S4). Because a hydrophobic transmembrane helix tends to tilt at a position of closely spaced Gly and Pro residues in the interior of the membrane, the PxxG motif could potentially contribute to the location of the C-terminal globular domain of ClsA in the cytoplasm. To examine the role of the PxxG motif for the flippability of ClsA, either P48 or G51 or both were substituted with Ala. These plasmid-borne ClsA (EE) derivatives synthesized almost the same amount of CL as ClsA (EE) in BKT12 cells (fig. S9A) and supported the Mg-dependent growth of PE-depleted cells (fig. S9B). ECAM showed that these ClsA (EE) derivatives displayed a dual topology in PE-deficient cells (Fig. 2G and fig. S9C). These results indicate that the conserved PxxG motif is not essential for both enzyme activity and topological duality of ClsA in PE-deficient cells.

The ability of ClsA to adopt an inverted topology correlates with cell viability of PE-deficient cells

If the generation of the inverted topology of ClsA is physiologically important, then the inability to adopt an inverted topology of ClsA would result in the loss of cell viability of PE-deficient cells. Because the C-terminal globular domain of ClsA should not be translocated across the IM without an associated TMD, we verified the requirement for the N-terminal TMDs to initiate a topological change in ClsA and to support cell viability of PE-deficient cells. However, it has been assumed that the N-terminal hydrophobic domain of ClsA is processed based on several observations. First, the apparent molecular weight of ClsA on SDS-PAGE was around 45 to 46 kDa (*7*, *20*, *45*) whereas the estimated molecular weight predicted from its amino acid sequence is 54.8 kDa. Second, the elimination of the N-terminal hydrophobic domains of ClsA did not disrupt its CL synthase activity both in vivo and in vitro whereas the elimination of the C-terminal domain of ClsA diminished enzymatic activity (*6*, *34*). Moreover, it was found that His_{10}-tagged ClsA at the N terminus could not bind to TALON metal affinity resin (*53*), whereas C-terminal tagged ClsA could bind to the column even though the latter construct was not active (*20*). Several attempts to determine the N-terminal sequence of purified ClsA by applying Edman degradation failed (*20*, *46*), suggesting that the N terminus of ClsA is blocked. We investigated whether the N terminus of ClsA undergoes post-translational processing or not. To monitor the processing of ClsA, an N-terminal T7 tag of 11 amino acids was added to full-length and each incrementally truncated ClsA (EE) derivative (Fig. 3A). Because the T7 tag does not have any net charge, it should not affect the membrane topology of hydrophobic TMDs. If the N terminus of ClsA is processed, then the processed protein should not be detected by an anti–T7 tag antibody but will be detected by an anti–EE tag antibody. To analyze all populations of ClsA (EE) and its T7-tagged derivatives, a total membrane fraction was prepared by high-speed ultracentrifugation (200,000*g*). All constructs with an inserted T7 tag at their respective N-termini positions were detected by an anti–T7 tag antibody (Fig. 3B and fig. S10), indicating that the N termini of all engineered constructs were not processed. It is noteworthy that all truncated constructs ran nearly similarly with full-length ClsA (EE) on SDS-PAGE (Fig. 3B and fig. S10), strongly indicating that processing of the N-terminal domain of ClsA cannot be determined from the apparent molecular weight of ClsA on SDS-PAGE as previously suggested. Phospholipid analysis of BKT12 expressing plasmid-borne T7-tagged ClsA (EE) revealed that only T7-Δ59-ClsA (EE) among these N-terminal truncated ClsA derivatives could make an equivalent amount of CL in comparison with amounts of CL synthesized by full-length ClsA (EE) (fig. S11), whereas substantial amounts of all ClsA derivatives were expressed and targeted to the IM (Fig. 3B). Thus, the T7-Δ59-ClsA (EE) construct could be instrumental in verifying whether the N-terminal TMDs are essential for the Mg-dependent growth of PE-deficient cells.

ECAM was performed to map the localization of T7-Δ59-ClsA (EE) in +PE and PE-depleted cells in the Δ*clsABC* background. T7-Δ59-ClsA (EE) was expressed in KS410, and cells were grown with (+PE) or without (PE-depleted) aTc inducer. In +PE cells, T7-Δ59-ClsA (EE) was only derivatized by AMS when cells were disrupted by

sonication (Fig. 3D), indicating that the catalytic domain of T7-Δ59-ClsA (EE) localizes to the cytoplasmic leaflet of the IM. Consistent with this result, T7-Δ59-ClsA (EE) is localized on the cytoplasmic leaflet of the IM in BKT12 (fig. S12A). T7-Δ59-ClsA (EE) was also not derivatized by externally added AMS under the PE-depleted conditions (Fig. 3E). The absence of labeling of intracellular cysteines of the nonintegral form of ClsA, even in the PE-depleted cells in the Δ*clsABC* background, confirmed that the IM is not permeable to AMS under our experimental conditions. These results indicate that the N-terminal two-TMD hairpin is essential for the generation of the inverted topology of ClsA (EE). We used this TMD-less "soluble" ClsA (EE) to test an intrinsic permeability of the IM to the thiol-specific labeling reagent AMS (Fig. 3C) in addition to the widely used cytosolic bacterial marker LacZ. To validate ECAM and test the permeability of the IM to AMS under the PE-depleted conditions, T7-Δ59-ClsA (EE) was expressed in KS310 outgrown under PE-depleted conditions. Because the Mg-dependent growth of KS310 was supported by chromosomal-borne non–EE-tagged ClsA, only T7-Δ59-ClsA (EE) can be immunodetected by an anti–EE tag antibody in Western blotting. We observed no derivatization of T7-Δ59-ClsA (EE) by externally added AMS even though PE was depleted (fig. S12B), confirming that the IM is not permeable to AMS and its integrity is not compromised under our experimental conditions. Furthermore, we asked whether T7-Δ59-ClsA (EE) can support divalent cation-dependent growth of conditionally lethal KS510 cells. Full-length ClsA (EE) supported the growth of KS510 as expected. However, T7-Δ59-ClsA (EE) was unable to phenocopy Mg-dependent growth of KS310 (Fig. 3F). We confirmed that almost the same level of CL was synthesized in KS410 expressing full-length and TMD-less ClsA (EE) (fig. S12C). These results show that the viability of PE-deficient cells is correlated with the ability of ClsA to adopt an inverted topology.

Formation of PM and DPM was still observed when BKT12 expressing T7-Δ59-ClsA (EE) were grown in the presence of 600 mM mannitol (fig. S13). Therefore, biosynthesis of PM and DPM is not a strong indicator of CL synthesis in the periplasmic leaflet of the IM as previously proposed (*19*).

CL accumulates on the cytoplasmic leaflet of the IM of PE-deficient cells expressing a TMD-less ClsA derivative

The fact that T7-Δ59-ClsA (EE) was unable to support Mg-dependent growth of PE-depleted cells strongly suggests that CL synthesized on the cytoplasmic leaflet of the IM cannot be translocated across the IM in sufficient amounts to support divalent cation-dependent growth of PE-deficient cells. If this is the case, then CL should accumulate on the cytoplasmic leaflet of the IM of T7-Δ59-ClsA (EE)–expressing cells. We took advantage of the CL-independent growth phenotype of strain UE91 (Δ*clsABC* Δ*pssA* P_{araBAD}-*pssA*) (fig. S2D). Either full-length ClsA (EE) or T7-Δ59-ClsA (EE) was expressed using the $P_{LtetO-1}$ promoter on a plasmid [pTet-ClsA (EE) or pTet-T7-Δ59-ClsA (EE)]. Although the amount of CL in a total phospholipid extract of UE91 expressing either ClsA (EE) or T7-Δ59-ClsA (EE) and outgrown without arabinose (e.g., under the low PE levels) was nearly the same (15%), the amount of CL in the IM of the cells expressing T7-Δ59-ClsA (EE) was 1.5-fold higher than that of full-length ClsA (EE)–expressing cells (Fig. 4A). The calculation of the mol % of each phospholipid (Fig. 4A, right) and ratiometric percent distribution of PG+CL/PE in whole cells and isolated IMs allowed us to approximate the apparent distribution of CL between the IM and OM (Fig. 4B). The ratio of PG+CL/PE was twofold lower in total cells but correspondingly higher in the IM of T7-Δ59-ClsA (EE)–expressing cells when compared with the IM of cells expressing full-length ClsA (EE) (first two bars in Fig. 4B). These results indicate that anionic phospholipids accumulate in the IM in T7-Δ59-ClsA (EE)–expressing cells. The CL/PE ratio in the IM of T7-Δ59-ClsA (EE)–expressing cells was also higher, but the PG/PE ratio in the IM of T7-Δ59-ClsA (EE)–expressing cells was the same as cells expressing full-length ClsA. These reciprocal distributions indicate that CL accumulates in the IM of T7-Δ59-ClsA (EE)–expressing cells.

To directly examine the accumulation of CL in the cytoplasmic leaflet of the IM in T7-Δ59-ClsA (EE)–expressing cells, the CL-specific probe EryA-EGFP was used. EryA-EGFP is composed of an N-terminal CL-binding peptide EryA and C-terminal EGFP. EryA-EGFP binds strictly to CL and does not bind to other anionic phospholipids such as PG or PA (*15*). The accumulation of CL on the cytoplasmic leaflet of the IM was examined by an EryA-EGFP cosedimentation assay with uniformly oriented inside-out membrane vesicles (ISOv) in which the outer leaflet of ISOv corresponds topologically to the cytoplasmic leaflet of the IM in living cells. The phospholipid composition of ISOv prepared from UE91 expressing either full-length ClsA (EE) or T7-Δ59-ClsA (EE) growing in the absence of arabinose is shown in fig. S14. These ISOv were incubated with purified EryA-EGFP for 30 min followed by collection of ISOv by ultracentrifugation. The amount of EryA-EGFP bound to the ISOv was quantified by measuring the fluorescence intensity of EryA-EGFP (fig. S15). The fluorescence intensity of EryA-EGFP bound to ISOv containing T7-Δ59-ClsA (EE) was about 2.5 times higher than the fluorescence intensity of ClsA (EE) containing ISOv (Fig. 4C), whereas the amount of total CL in T7-Δ59-ClsA (EE) IMs was only 1.3 times higher than that of ClsA (EE) IMs (fig. S14). The same results were obtained when EryA-EGFP bound to ISOv was subjected to SDS-PAGE and immunoblotting (Fig. 4D). These results indicate that CL accumulates predominantly on the cytoplasmic leaflet of the IM of cells expressing T7-Δ59-ClsA (EE).

Introduction of negatively charged Glu residues downstream of second TMD results in reorientation of the adjacent globular domain to the periplasm in +PE cells

The membrane topology of most multispanning membrane proteins can be predicted following the experimentally proven positive-inside rule that states that the positively charged residues are overrepresented in EMDs on the cytoplasmic side of the membrane where they have been found statistically four times more abundant (*35*, *36*). ClsA has five positively charged residues and two negatively charged amino acids in the linker region that connects the second TMD and the catalytic globular domain, resulting in a +3 net charge in the linker region (Fig. 5A and fig. S4). Thus, a net positive charge in proximity to the second TMD might prevent the translocation of the following C-terminal globular domain to support the $ClsA_{cyto}$ topology in +PE cells. Although the positive-inside rule discounts the importance of negatively charged amino acid residues, their topological effect is observed when they are present in high numbers (*54*) or are properly located within a "window" region of seven residues from a TMD (*55*, *56*). The topologies of the N-terminal six-TM helical bundle of lactose permease LacY (*40*, *42*) and the N-terminal two-TMD hairpin of phenylalanine permease (PheP) (*51*) and γ-aminobutyrate permease (GabP) (*57*) are inverted relative to the membrane bilayer when assembled in membranes lacking PE. LacY also can be forced to flip even in wild-type cells by an increase in the net negative

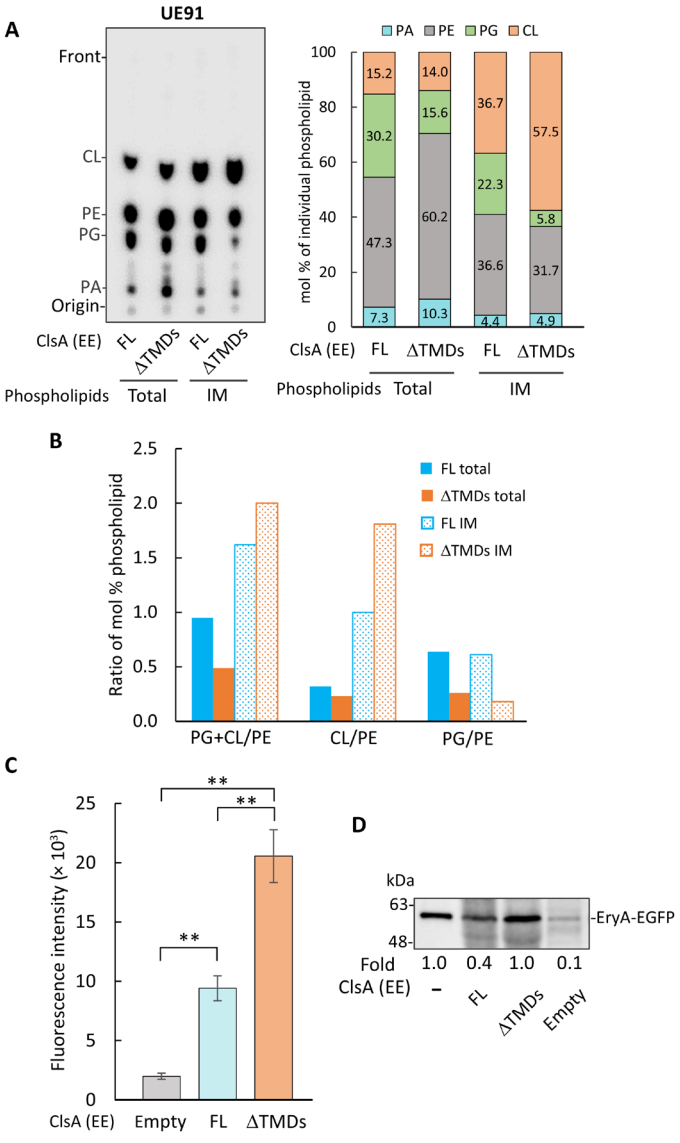

Fig. 4. Accumulation of CL on the cytoplasmic leaflet of the IM in low PE cells expressing TMD-less ClsA. (**A**) Phospholipid composition of whole cells (total) or IM fractions. UE91 harboring pTet-ClsA (EE) or pTet-T7-Δ59-ClsA (EE) was grown with 50 mM $MgCl_2$ and aTc (100 ng/ml). Phospholipids were uniformly labeled with [^{32}P]PO_4 (1 μCi/ml). Phospholipids were extracted either from whole cells or the IM fraction prepared as described in the Materials and Methods. Individual phospholipids were separated by TLC with solvent 2. The mol % of individual phospholipids is indicated in the right panel. (**B**) The ratiometric percent distribution of "PG+CL/PE," "CL/PE," and "PG/PE" in whole cells and isolated IMs was calculated from (A). (**C** and **D**) EryA-EGFP co-sedimentation assay with ISOv. ISOv prepared from the indicated strain were used for the assay. The amount of EryA-EGFP bound to the ISOv was detected either by Typhoon FLA 9500 (C) or Western blotting (D). Fluorescence intensity of EryA-EGFP was quantified by ImageQuant (C). Three individual experiments were done, and the average values are indicated together with the SD. The *P* values were determined from three individual experiments. $^{**}P < 0.01$. The intensity of EryA-EGFP bound to ISOv upon Western blotting was quantified by AzureSpot Pro and normalized using 50 ng of purified EryA-EGFP loaded in lane 1 (D).

charges in the EMDs residing in the cytoplasm (*41*). These observations indicate that not only positively charged residues but also negatively charged residues can act as a topogenic signal by attenuating the retention signal of positively charged residues. Although the

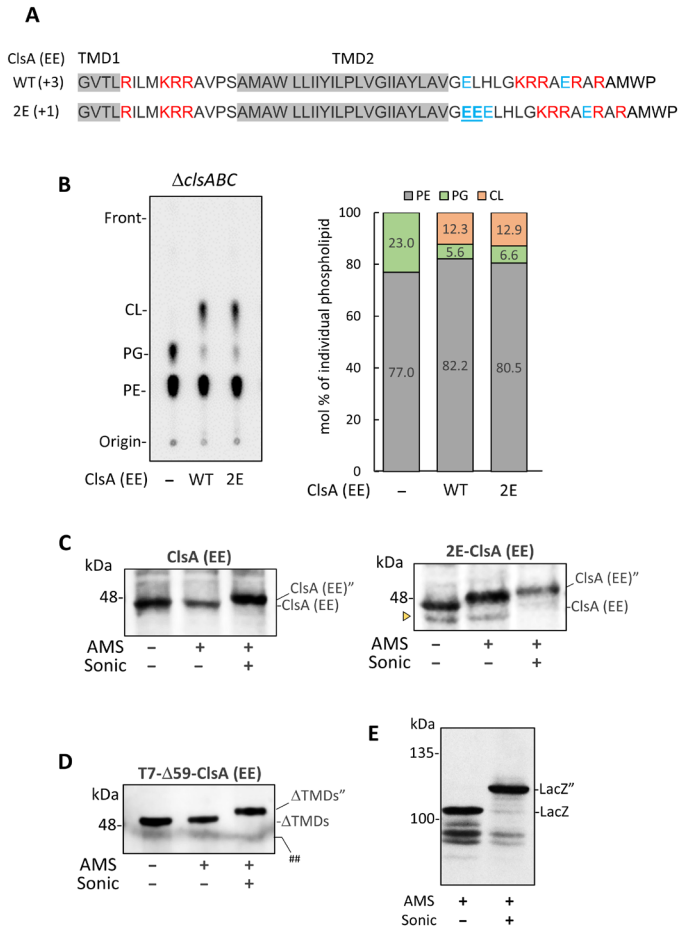

Fig. 5. Topological inversion of ClsA by introducing multiple Glu residues. (**A**) Amino acid sequence of ClsA upstream and downstream of TMD2. TMD is highlighted in gray. Blue and red characters indicate negatively and positively charged amino acids, respectively. The name of each mutant and net charge in the following region of TMD2 are shown on the left. (**B**) KS410 harboring pBAD18-ClsA (EE) or pBAD18-2E-ClsA (EE) were grown in LB medium with 0.2% arabinose and aTc (100 ng/ml) until OD_{600} 0.6–0.8. Phospholipids were uniformly labeled with [^{32}P]PO_4 (1 μCi/ml). Extracted phospholipids were separated by solvent 1 and then detected by Phosphoimager and quantified by ImageQuant. The mol % of individual phospholipids is indicated in the lower panel. (**C** and **D**) Cells grown as in (B) were subjected to ECAM. AMS-derivatized ClsA (EE) and T7-Δ59-ClsA (EE) are indicated as ClsA (EE)" (C) and ΔTMDs" (D), respectively. The potential product of degradation is indicated by a yellow triangle. (**E**) KS410 harboring pBAD18-2E-ClsA (EE) were grown as described in the legend to (B). Intact or disintegrated cells were incubated with 1 mM AMS for 60 min, imitating the conditions for the ClsA ECAM experiments. Intact cells were disintegrated by ultrasonication, and the cytoplasmic fractions were retained after removal of the membrane fraction by ultracentrifugation (200,000*g*) for subsequent SDS-PAGE and Western blotting with anti-LacZ monoclonal antibodies.

positive-inside bias is pronounced in ClsA, we decided to verify whether the thermodynamic disadvantage of translocation to the periplasm of the highly positively charged region adjacent to the second TMD and the following large globular domain can be overridden even in the presence of a wild-type amount of PE. Two negatively charged Glu residues were introduced between G59 and E60 residues (Fig. 5A, 2E-ClsA) to eliminate the strong topological retention signal and enforce a negative outside bias within the spacer domain linking the large hydrophilic globular domain to the second TMD. 2E-ClsA

(EE) was able to synthesize a comparative amount of CL compared to ClsA (EE) in a Δ*clsABC* strain when overproduced from a plasmid (Fig. 5B). To examine the membrane topology of 2E-ClsA (EE) derivative, ECAM was performed. As shown in Fig. 5C, wild-type ClsA (EE) was not derivatized by externally added AMS. However, we observed that 2E-ClsA (EE) was fully derivatized by externally added AMS, indicating that engineered 2E-ClsA (EE) uniformly adopts an inverted $ClsA_{peri}$ topology even in +PE cells. In 2E-ClsA (EE)–expressing cells, the residual potential degradation product running below the immunoreactive band of ClsA (EE) derivatives appeared, which was not observed in wild-type ClsA (EE)–expressing cells (Fig. 5C indicated by a yellow triangle). This potential degradation product was not derivatized by externally added AMS but fully derivatized when membranes were disrupted (Fig. 5C), indicating that the product resides in the cytoplasm. T7-Δ59-ClsA (EE) (Fig. 5D) and LacZ (Fig. 5E) were not derivatized by externally added AMS, indicating that AMS does not penetrate the IM of intact cells under our experimental conditions. These results indicate that the introduction of negatively charged Glu residues in the linker region promotes the translocation of the following globular domain of ClsA into the periplasm and forces this protein to adopt a uniform $ClsA_{peri}$ topology in +PE cells.

Two-TMD hairpin of ClsA has structural information for the generation of inverted ClsA in PE-deficient cells

All data presented above indicate that the amount of PE sets the threshold level for the flippability of ClsA, and the two N-terminal TMDs are essential for the generation of an inverted topology. These data provoked us to determine whether replacing the two-TMD hairpin of ClsA with the two-TMD hairpin that intrinsically adopts an N-out/C-out topology can override the lipid bilayer constraints and strong retention bias attributed to multiple positively charged residues in the spacer region that ensured cytoplasmic residency of the C-terminal catalytic globular domain of ClsA in +PE cells. The leader peptidase (LepB) is an essential membrane protein that could serve as instructive model when considering ClsA orientation because N-terminal two TMDs of LepB adopt an N-out/C-out topology and its C-terminal catalytic globular domain orients permanently into periplasmic space (Fig. 6A). To examine whether two-TMD hairpin of LepB can force the globular domain of ClsA to flip, both TMDs of ClsA (1 to 59) were substituted with the N-terminal two TMDs of leader peptidase (LepB) (Fig. 6B). Considering that introduction of positively charged amino acid within a window of 30 amino acids following the second TMD of LepB prevents translocation of the following globular region (*58*), the chimeric constructs with either two TMDs (1 to 77; LepB+0) or two TMDs with the following downstream LepB region (1 to 117; LepB+40) were successfully engineered (Fig. 6B). We found that the swapping of TMDs (LepB+0) resulted in interference of CL synthesis activity in vivo (Fig. 6C). Further extension of the LepB region following the two-TMD hairpin (LepB+40) diminished CL synthesis activity (Fig. 6C), indicating that inherent TMDs of ClsA are important for catalytic activity of the C-terminal globular domain. To examine whether the N-out/C-out orientation of LepB TMDs can force the translocation of the globular domain of ClsA (EE) even in +PE cells, ECAM experiments were performed. LepB+0-ClsA (EE) migrated as a 55-kDa protein (indicated as a blue triangle in Fig. 6D) in accordance with the predicted molecular weight along with a faster migrating band that runs around 46 kDa (indicated as a yellow triangle in Fig. 6D). In LepB+40-ClsA (EE)–expressing cells, only the faster migrating band was observed (Fig. 6D). Given that all incrementally truncated ClsA (EE) derivatives including the TMD-less version migrated around 46 kDa (Fig. 3B and fig. S10), it is reasonable to suggest that the faster migrating band represents the C-terminal globular domain in which the N-terminal LepB TMDs were removed. All LepB chimeric constructs were not derivatized by externally added AMS unless cells were broken by sonication (Fig. 6E), indicating that the globular domain of these derivatives resides on the cytoplasmic side of the IM. Next, we examined whether the LepB+0-ClsA (EE) chimeric protein can adopt an inverted topology in PE-deficient cells. LepB+0-ClsA (EE) was expressed in KS410, and ECAM was performed under the PE-depleted conditions. We observed that LepB+0-ClsA (EE) was not able to adopt an inverted topology (Fig. 6F). These results indicate that the TMDs of LepB cannot substitute for functionally and structurally important native ClsA TMDs and promote periplasmic residence of the globular domain of ClsA even though the essential membrane protein LepB TMDs adopts an N-out/C-out topology.

Osmotic down-shock induces inversion of ClsA in +PE cells

There is a correlation between the generation of the inverted topology of ClsA and cell viability of PE-deficient cells. However, is the generation of inverted ClsA a specific phenomenon observed only in genetically manipulated PE-deficient cells or does ClsA have the capacity to reorient itself if the membrane phospholipid composition is not changed? Does this ever happen in a normal *E. coli* cell with wild-type PE levels around 70 to 75% of all phospholipids? Because the cellular amount of CL varies in response to the extracellular osmolality (*5*, *59*), we examined the orientation of the catalytic domain of ClsA relative to the membrane bilayer within the IM of *E. coli* cells challenged by chronic and acute changes in extracellular osmolality. We confirmed that another nonspecific band close to ClsA (EE) did not appear under the osmotic stress conditions in ClsA (EE)–expressing cells (fig. S16). BKT12 expressing ClsA (EE) were grown in LB medium either in the presence of 0.5 M NaCl (LB/0.5 M NaCl medium) or in the absence of NaCl (saline-less TY medium) until the mid-log phase followed by assessment of the topology of ClsA (EE) by ECAM. Derivatization of ClsA (EE) by externally added AMS was not observed under both conditions (Fig. 7A), indicating that the ClsA globular domain faces the cytoplasm. Next, we examined the effect of an acute increase (up-shock) or decrease (down-shock) in environmental osmolality on the topology of ClsA. The ClsA (EE) globular domain remained facing the cytoplasm when cells were subjected to osmotic up-shock. On the other hand, we observed that externally added AMS derivatized a substantial amount of ClsA (EE) when cells were challenged to osmotic down-shock (Fig. 7B, upper panel versus lower panel), resulting in a shift in mobility of the protein on SDS-PAGE. When cells were grown for 90 min after osmotic down-shock, the inverted ClsA (EE) was no longer observed (Fig. 7C), suggesting that the generation of inverted ClsA (EE) upon osmotic down-shock was temporary. In contrast to full-length ClsA (EE), nonderivatized TMD-less T7-Δ59-ClsA (EE) remains on the cytoplasmic leaflet of the IM even after osmotic down-shock (Fig. 7D), indicating that N-terminal TMDs are essential for the generation of an inverted topology in +PE cells, and AMS does not across the IM under our conditions.

To examine the physiological significance of the generation of inverted ClsA upon osmotic down-shock, wild type, BKT12, and BKT12 expressing either full-length or TMD-less ClsA (EE) grown

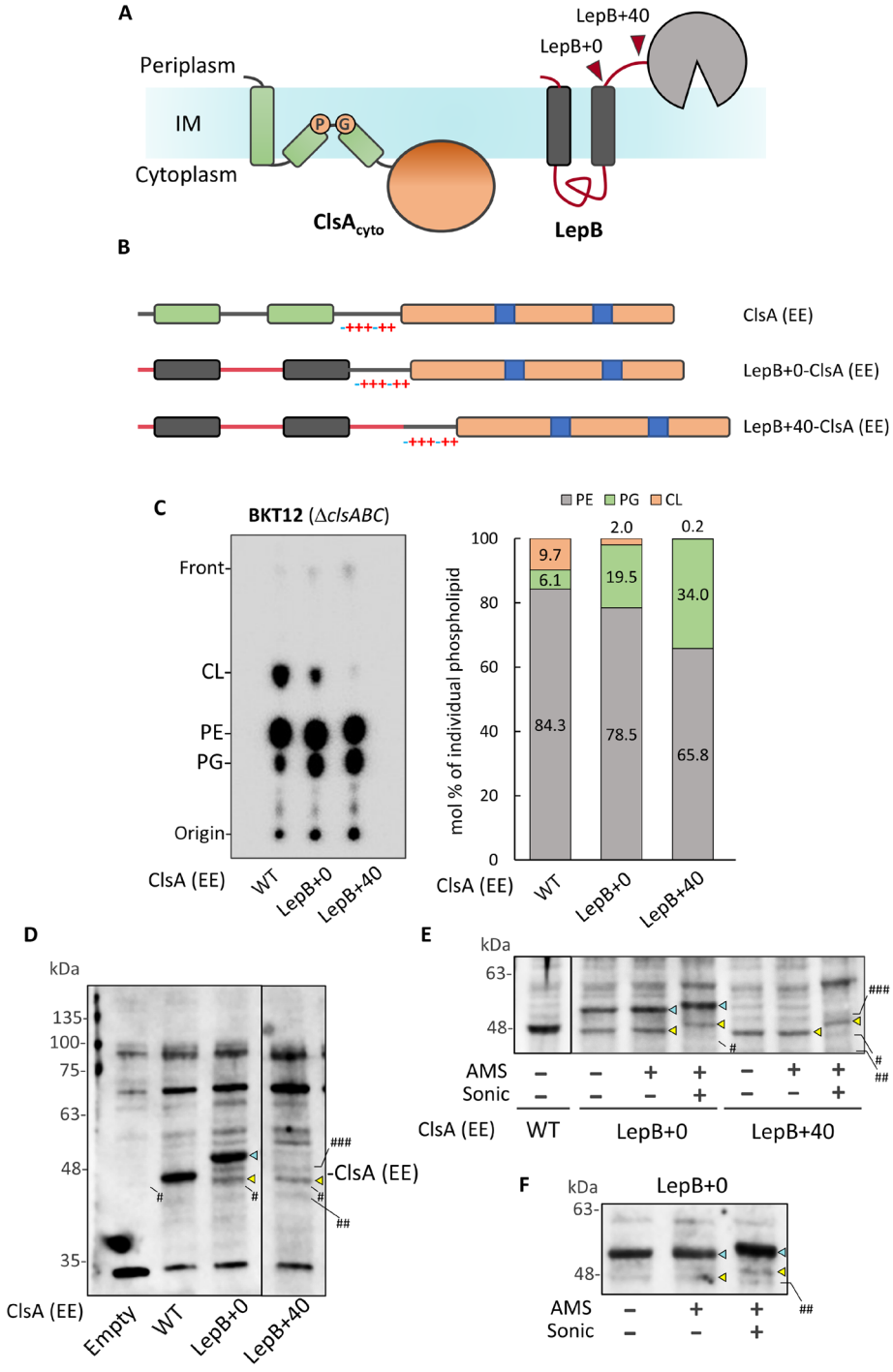

Fig. 6. Replacing the TMDs of ClsA with the TMDs of LepB. (**A**) Schematic representation of the membrane topology of $ClsA_{cyto}$ and LepB. Either two TMDs (1 to 77; LepB+0) or two TMDs followed by the downstream sequence of LepB (1 to 117; LepB+40) were used to construct the LepB-ClsA chimeric proteins. (**B**) Schematic representation of LepB-ClsA (EE) chimeric proteins. Two TMDs and the hydrophilic extramembrane region of ClsA are shown as green boxes and a black line, respectively. The C-terminal globular domain of ClsA is shown as orange boxes with blue boxes corresponding to the two HKD motifs of ClsA. Two TMDs and adjacent hydrophilic extramembrane in the region of LepB are shown as black boxes and a red line, respectively. (**C**) TLC analysis of the phospholipid composition. BKT12 harboring pBAD18-ClsA (EE), pBAD18-LepB+0-ClsA (EE), or pBAD18-LepB+40-ClsA (EE) were grown in LB medium with 0.02% arabinose and [^{32}P]PO_4 (1 μCi/ml). Extracted phospholipids were separated by solvent 2 and then detected by Phosphoimager and quantified by ImageQuant. The mol % of individual phospholipids is indicated in the right panel. (**D**) Immunoblot analysis of the LepB-ClsA (EE) chimeric protein. BKT12 harboring empty vector, pBAD18-ClsA (EE), pBAD18-LepB+0-ClsA (EE), or pBAD18-LepB+40-ClsA (EE) were grown with 0.02% arabinose. Ten micrograms of the membrane fraction was subjected to SDS-PAGE/immunoblotting. (**E** and **F**) Membrane topology of the LepB-ClsA (EE) chimeric protein. BKT12 grown as described in (D) were subjected to ECAM (E). KS410 harboring pBAD18-Lep+0-ClsA (EE) grown under the PE-depleted conditions was subjected to ECAM (F).

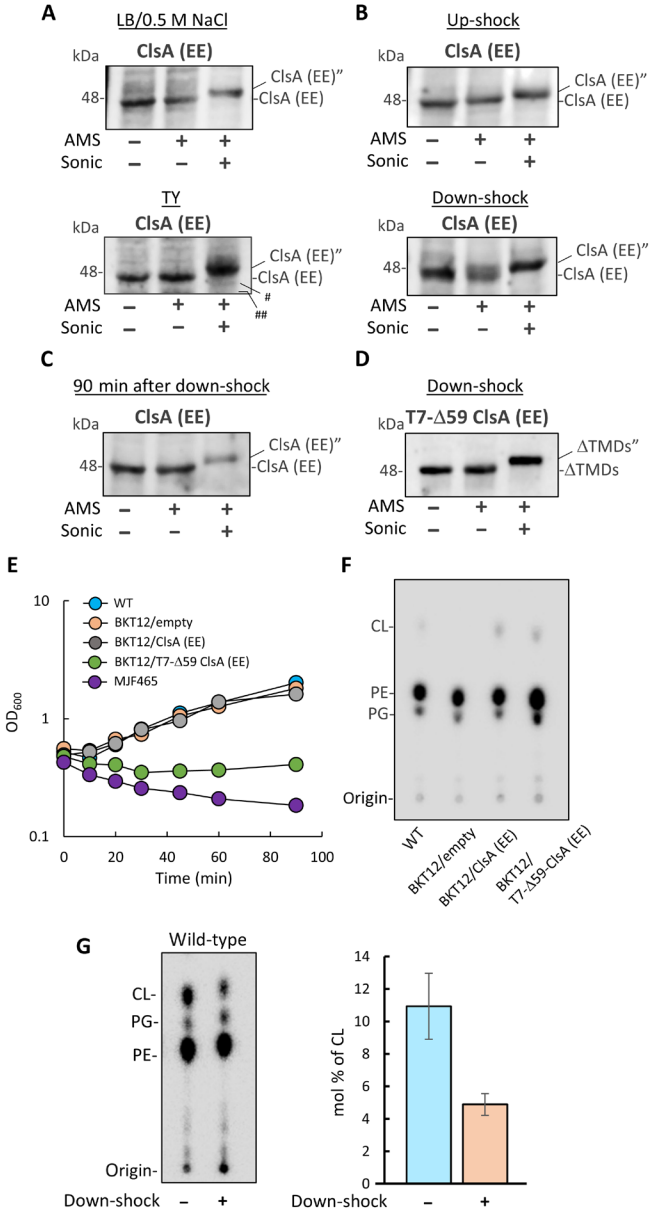

Fig. 7. Topological duality and flipping of ClsA in +PE cells. (**A**) Effect of extracellular osmolality on the membrane topology of ClsA. BKT12 harboring pBAD18-ClsA (EE) were grown either in LB/0.5 M NaCl or saline-less TY medium, following assessment of the membrane topology of ClsA (EE) by ECAM. Expression of ClsA (EE) was induced by addition of 0.02% arabinose to the growth medium. (**B**) Effect of acute change in osmolality on the membrane topology of ClsA. BKT12 harboring pBAD18-ClsA (EE) were grown in LB for osmotic up-shock or in LB/0.5 M NaCl for osmotic down-shock. Osmotic up-shock and down-shock were performed as described in the Materials and Methods. (**C**) BKT12 harboring pBAD18-ClsA (EE) were grown in LB/0.5 M NaCl until the cell density reached OD_{600} 0.2 to 0.3. After collecting cells by centrifugation, the osmotic down-shock was performed by resuspending in TY medium. After growing for another 90 min, the membrane topology of ClsA was assessed by ECAM. (**D**) Role of N-terminal TMDs in generating inverted ClsA upon osmotic down-shock. BKT12 harboring pBAD18-T7-Δ59-ClsA (EE) were grown in LB/0.5 M NaCl with 0.02% arabinose. Osmotic down-shock and ECAM were performed as described in the Materials and Methods. (**E**) Role of the N-terminal TMDs in cell survival after osmotic down-shock. Indicated cells were grown in LB/0.5 M NaCl until the cell density reached OD_{600} 0.6. Cells were collected by centrifugation and then resuspended in TY medium. OD_{600} was measured at the indicated time point. ClsA (EE) and T7-Δ59-ClsA (EE) were induced by adding 0.02% arabinose to the growth medium. The same results were obtained from two individual experiments, and representative results are shown. (**F**) Phospholipid composition in osmotic down-shock stressed cells. Indicated strains were grown and subjected to osmotic down-shock as described in Fig. 6E. [^{32}P]PO_4 (1 μCi/ml) was added when cells were resuspended into TY medium, followed by growth for another 30 min. Extracted phospholipids were separated by solvent 2, and then detected by Phosphoimager. (**G**) Suppression of CL synthesis in osmotic down-shock stressed cells. Wild-type cells were grown in LB medium containing 0.5 M NaCl until the cell density reached OD_{600} 0.3. After dividing samples into two equal aliquots, one was resuspended in isotonic LB/0.5 M NaCl medium, and another was resuspended in a low-salinity TY medium. Phospholipids were labeled by adding [^{32}P]PO_4 (10 μCi/ml) for 1 min. Metabolic phospholipid labeling was stopped by adding a potassium phosphate buffer (10 mM final concentration), followed by a 15-min chase. Extracted phospholipids were separated by solvent 1 and then detected by Phosphoimager and quantified by ImageQuant. The mol % of CL is indicated in the right panel. Three independent experiments were performed, and the average values are indicated together with the SD.

in LB/0.5 M NaCl medium were challenged to osmotic down-shock by resuspension in low-osmotic saline-less TY medium. Although wild type and BKT12 resumed growth within 20 min after osmotic down-shock, we observed that the growth of BKT12 expressing T7-Δ59-ClsA (EE), but not full-length ClsA (EE), was arrested upon osmotic down-shock (Fig. 7E). The acute drop in environmental osmolality of the cells results in an influx of water that induces the expansion of the cell envelope. The resulting increased IM tension is thought to activate the nonspecific export of solutes through mechanosensitive channels, which act as biological emergency release valves that allow cytoplasmic solutes to be ejected rapidly from the cell and release the pressure built up by hypoosmotic shock to prevent cells from rupture (*60*). We observed that MJF465, where three abundant mechanosensitive channels (MscS, MscL, and MscK) are disrupted, could not resume growth after osmotic down-shock similarly to BKT12 expressing T7-Δ59-ClsA (EE) (Fig. 7E). We confirmed that PE was the most abundant phospholipid synthesized in osmotic down-shock stressed cells (Fig. 7F). Although CL synthesis is enhanced in LB/0.5 M NaCl medium, the CL biosynthesis or its turnover was suppressed or stimulated respectively by osmotic down-shock (Fig. 7G), suggesting that cells are trying to reduce the CL level in response to acute decrease in osmolality.

DISCUSSION

In this study, conditionally lethal mutants were successfully engineered and used as a model system in which the nonbilayer-prone formation of Mg-chelated CL on the periplasmic leaflet of the IM or OM is essential for cell viability in the absence of the most abundant nonbilayer-prone lipid. We established that the C-terminal globular catalytic domain of ClsA uniformly resides on the cytoplasmic side of the IM in PE-containing cells. Unexpectedly, the catalytic domain of ClsA displays a dual topology when PE is limiting (Fig. 2, C and D). However, when two membrane-anchoring N-terminal TMDs of ClsA were removed, ClsA was able to synthesize the same amount of CL as the full-length ClsA (figs. S11 and S12C) but did not support the divalent cation-dependent growth of PE-deficient cells (Fig. 3F) and accumulated CL on the cytoplasmic leaflet of the IM (Fig. 4, C and D). This TMD-less ClsA was still IM-associated with its catalytic domain facing the cytoplasm in PE-depleted conditions (Fig. 3E), indicating that the TMDs are essential for flipping the catalytic globular domain to the periplasmic side of the IM. From these observations, we propose that inverted ClsA serves as a primary pathway for supplying CL on the periplasmic leaflet of the IM in PE-deficient cells.

We further extended our finding on the organization of a dual topology of ClsA in genetically manipulated PE-deficient cells to gain insight into whether ClsA can adopt a dual topology in the cells containing wild-type levels of PE to establish physiological relevance. We demonstrated that the globular domain of ClsA is temporarily exposed to the periplasm in response to a sudden decrease in osmolality, even in the cells containing a wild-type amount of PE (Fig. 7B versus Fig. 7C). The physiological importance of CL itself or regulation of the ratio of PG/CL for cell survival after downward shift in external osmolality has been missed presumably because the growth defect upon osmotic down-shock was not observed in BKT12 (*clsABC* null strain) (Fig. 7E). In contrast to the robust growth of BKT12 after osmotic down-shock, the expression of T7-Δ59-ClsA (EE), but not full-length ClsA (EE), inhibited cell growth (Fig. 7E). Given that BKT12 were able to grow as well as a wild type after osmotic down-shock, it would be better to think that the pre-existing adaptive increase in the amount of PG in BKT12 can fully substitute the requirement of the CL on the periplasmic leaflet of the IM. On the other hand, intensive CL synthesis on the cytoplasmic leaflet of the IM by T7-Δ59-ClsA (EE), resulting in the consumption of PG and accumulation of CL in the inner leaflet, would be more harmful than the absence of CL. Consistent with these ideas, CL synthesis was suppressed upon osmotic down-shock (Fig. 7G). From these results, we conclude that topological rearrangement of ClsA during osmotic down-shock is one of the mechanisms to avoid intensive synthesis and accumulation of CL on the cytoplasmic leaflet of the IM, which is further evidenced in the experiment with a fully active soluble nonintegral form of ClsA.

Osmotic stress is one of the most common environmental stressors. A rapid and acute decrease in external osmolarity is a viability-threatening change that requires a rapid adaptation for a single-celled enteric bacterium, which regularly faces drastic changes in its osmotic microenvironment, including entry and exit from the intestine and the transition of pathogens from mammalian hosts to fresh water (*61*, *62*). When bacteria are challenged with an osmotic down-shock, turgor increases within milliseconds due to fast water influx into the cytoplasm, resulting in temporal cell volume expansion (*63*). The increase in the tension of the IM activates mechanosensitive channels that release solutes rapidly to the outside of the cells, resuming the original cell volume and turgor pressure (*63*) to protect cells from rupture (*60*). The growth defect observed in BKT12 expressing T7-Δ59-ClsA (EE) upon osmotic down-shock is like that in cells with three disrupted abundant mechanosensitive channels (Fig. 7E). MscS gates more frequently in the presence of CL and ultimately destabilizes the open state of MscS in a dose-dependent manner, suggesting that its closed state may be stabilized by CL (*64*). Thus, the imbalance of the local or global transmembrane distribution of PG and CL across the IM will need to be considered to understand the growth defect of BKT12 expressing T7-Δ59-ClsA (EE) under osmotic down-shock stress conditions and the role of CL in the function of mechanosensitive channels.

What regulatory mechanism determines the fate of membrane topogenesis of ClsA? The most straightforward interpretation of the organization of ClsA dual topologies is that changes in the PE level destabilize the structure of ClsA and remove the protein structure from equilibrium. In +PE cells, the native topology of ClsA is stabilized by an energy valley and is separated from the inverted state by a free-energy barrier (black line in Fig. 8). Thus, ClsA preferably adopts the $ClsA_{cyto}$ topology required for CL synthesis on the cytoplasmic leaflet of the IM. The absence of PE alters the energy landscape of ClsA (orange line in Fig. 8), so inverted topologies become energetically favorable. Subsequent folding events for each intermediate topomer would then impose a high activation energy and thermodynamically block interconversion between the two conformations, resulting in stable dual conformations of ClsA within the same membrane. However, the ΔG activation free-energy barrier must be overcome to invert ClsA in +PE cells. A single-cell imaging analysis observed temporal expansion of cell volume upon osmotic down-shock, resulting in elongation of cell length (*63*). This change in cell volume should increase the IM elastic tension due to cell swelling. The potential change in physical properties of the membrane in response to osmotic down-shock could change the transition state of the free-energy barrier, which prevents flipping in +PE cells (dashed line in Fig. 8). The change

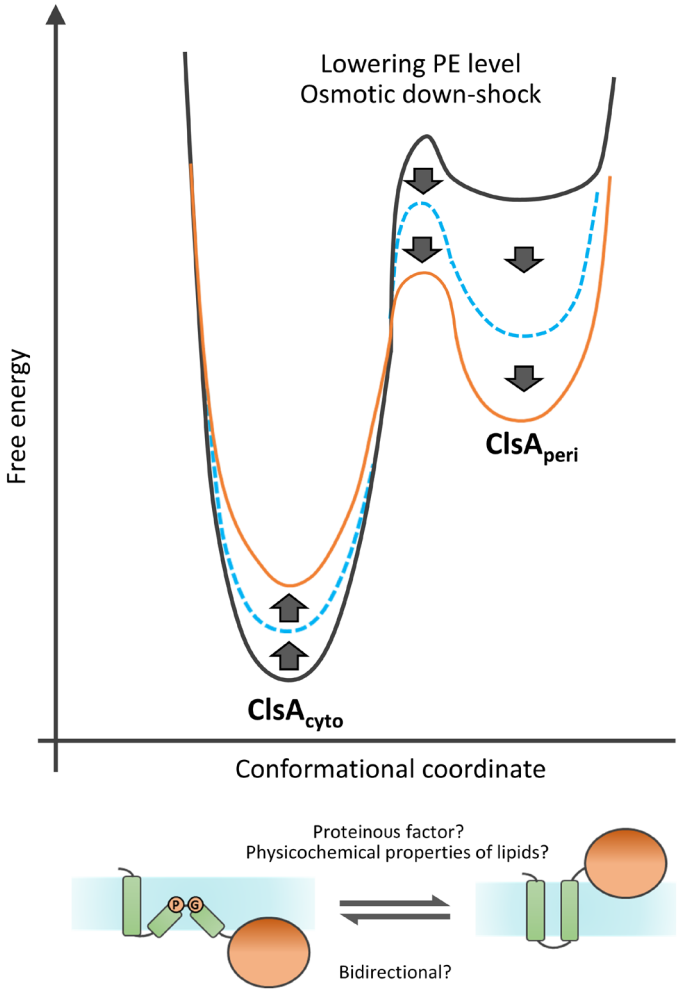

Fig. 8. PE and IM in-plane tension set a threshold level for flippability of ClsA. The dual-minima free energy landscape (funnel shape) reshaping for topogenesis of ClsA by changes in lipid composition and IM tension is shown. The topological ClsA heterogeneity can arise and disappear simply through perturbations of lipid- and membrane tension–sensitive kinetic and thermodynamic equilibria. Alternatively, the equilibrium could be shifted in favor of one of the topologies independently of the PE level by engineering new topogenic elements within the protein structure (Fig. 5).

in the thermodynamic landscape and reshaping and smoothing of the energy funnel shape would result in stable dual conformations of ClsA within the same membrane. Because we observed that inverted ClsA was generated upon osmotic down-shock and disappeared after resuming cell growth (Fig. 7, B and C), it can be assumed that ClsA adopts the original ClA$_{cyto}$ topology following adaptation where the cell resumes its original cell volume and turgor pressure recovery. ClsA localizes to the cell poles where anionic phospholipids are concentrated (*20*, *65*, *66*). The lipid environment surrounding ClsA would contain a lower amount of PE, which could facilitate the generation of inverted ClsA even in +PE cells. However, given that inverted ClsA (EE) was not observed in the cells grown in a high-osmotic medium (Fig. 7A) where more anionic phospholipids appear to be concentrated at the cell poles (*65*), the PE-less environment at cell poles is insufficient to induce the inversion of ClsA. These observations suggest the change in physical and packing properties of the IM upon osmotic down-shock and PE-less lipid environment at cell poles cooperatively lower the energy barrier for transmembrane reorientation of ClsA in the presence of physiological amounts of PE.

We successfully engineered inverted ClsA in +PE cells by introducing two Glu residues juxtaposed to the end of the second TMD. These changes were sufficient to override the retention signal attributed to the presence of a highly positively charged cluster region (Fig. 5C) defining the localization of the catalytic globular domain of ClsA in the cytoplasm in +PE cells. Because engineered 2E-ClsA (EE) resulted in a uniformly inverted ClsA$_{peri}$ topology, the multiple Glu residues close to the second TMD dominantly determine the final topology of ClsA by acting as strong translocation signals or effectively attenuate the downstream located translocation retention signals as reported previously (*54*–*56*). These results clearly show that ClsA has an intrinsic ability to adopt different topologies and suggest that the presence of both positively and negatively charged residues downstream of TMD2 contributes to the flexibility of the membrane topology of ClsA. We also examined the role of N-terminal TMDs in the generation of inverted ClsA in PE-deficient cells by replacing them with two TMDs of LepB facing permanently its catalytic domain into the periplasm. The chimeric construct did not force the flipping of the C-terminal catalytic globular domain of ClsA even under PE-depleted conditions (Fig. 6, E and F). Thus, the essential information for the generation of inverted ClsA must be encoded in TMDs of ClsA.

We previously demonstrated that the membrane topology of the first half of LacY can be inverted in vivo by depletion of PE and corrected by introducing PE in a postinsertional manner (*40*, *41*). Such flip-flop requires no additional accessory proteins (*42*, *43*). Thus, folding and topogenesis of LacY in the membrane follow a thermodynamically driven route and can be rerouted by changing the surrounding lipid environment. On the other hand, whether the reorientation of the ClsA catalytic globular domain depends on protein components is still unknown. Whether preexisting ClsA synthesized in +PE cells can flip postinsertionally upon depletion of PE or osmotic down-shock is also unknown. Because it is hard to imagine that a large C-terminal globular domain of ClsA is translocated across the IM spontaneously even if the globular domain is fully unfolded as PE is decreased, another cellular factor might be recruited to facilitate inversion. Such accessory proteins can potentially pull apart the ClsA globular polypeptide chain, bringing it uphill on an energy landscape out of the low-energy minimum trap and then letting the protein go down to another energy minimum of the non-native inverted state (Fig. 8). The general SecYEG/SecA protein translocation machinery and the twin-arginine translocase (TAT) system could be somehow involved in generation of the topological duality of ClsA. However, the question remains how these proteinoid components are recruited to actively translocate the globular domain of ClsA only when PE is limited or the cells are challenged by osmotic down-shock. It is also unlikely that the TAT system is engaged in the generation of inverted ClsA because TMDs of ClsA do not contain conserved consensus TAT signal sequences, and we previously demonstrated that the TAT system is inactive in PE-deficient cells (*67*).

Although we proposed that CL can be directly supplied by inverted ClsA on the periplasmic leaflet of the IM in low PE and PE-deficient cells, how CL can reach the periplasmic leaflet of the IM in +PE cells is still unknown. Because catalytic sites of all three Cls enzymes are oriented toward the cytoplasm, there may be multiple pathways to deliver CL to the periplasmic side of the IM. Several models of the transmembrane movement of CL across IM in *E. coli* can be considered. The

transmembrane movement of CL could be driven by proteinoid components. Previously, it was reported that an *msbA* (A207T) temperature-sensitive mutant accumulated lipid A and phospholipid in the IM (*16*), suggesting that MsbA can facilitate the transmembrane movement of phospholipid across the IM. Recently, it was reported that PetA, which belongs to the DedA superfamily, facilitates the transmembrane movement of PE across the cytoplasmic membrane of *Bacillus subtilis* (*68*). *E. coli* has eight proteins that belong to the DedA superfamily (*69*), suggesting that these proteins are physiologically important. Nonspecific scrambling activity of membrane proteins have been reported (*70*, *71*), suggesting the existence of noncanonical families of lipid translocators. Although further investigations must be done, these subsets of membrane proteins could specifically or nonspecifically be involved in the protein-driven transmembrane movement of CL. Plant pathogen Xanthomonas expresses a bifunctional CL/PE synthase encoded by the *xc_0186* gene that has an N-terminal signal sequence (*72*) and therefore may use a conventional SecYEG/SecA translocon-dependent pathway for its passage into the periplasm to synthesize CL on the periplasmic leaflet of the IM. Some bacteria might have unique pathways to synthesize or deliver CL to the periplasmic leaflet of the IM. Although these potential mechanisms could facilitate the transmembrane movement of CL across the IM, the accumulation of CL on the cytoplasmic leaflet of the IM in T7-Δ59-ClsA (EE)–expressing cells (Fig. 4) and inability of two TMD-less ClsA to support Mg-dependent growth of PE-deficient cells (Fig. 3F) suggest that these potential protein-driven or spontaneous pathways are not effective enough to supply adequate amounts of CL to the periplasmic leaflet of the IM in PE-deficient cells or those potential pathways are dependent on the presence of PE. Thus, not only PE-deficient cells but also other strains with altered and finely tuned lipid composition will be an attractive genetic tool to identify the putative flippase and scramblase candidates.

MATERIALS AND METHODS

Materials

The *E. coli* strains (table S1), plasmids (table S2), and primers (table S3) used in this study are listed in Supplementary Materials and Methods. Antibody against the EE tag was purchased from Cell Signaling Technology. Antibody against the T7 tag was purchased from Bioss Antibodies. Antibody toward EGFP and AMS were purchased from Invitrogen. Monoclonal antibody against LacZ was purchased from Sigma-Aldrich. Silica gel thin-layer chromatography (TLC) plates were purchased from Merck. [^{32}P]PO_4 was obtained from PerkinElmer Inc. Mini-PROTEAN TGX precast gels were obtained from Bio-Rad. SuperSignal West Pico PLUS Chemiluminescent Substrate was obtained from Thermo Fisher Scientific.

Growth of bacteria

The rich medium for the growth of cells in either liquid culture or on agar plates was LB medium (10 g of Bacto Tryptone, 5 g of Bacto Yeast extract, and 5 g of NaCl/liter). Low-salinity TY medium is composed of 10 g of Bacto Tryptone and 5 g of Bacto Yeast Extract/liter. Media were supplemented with ampicillin (50 μg/ml), spectinomycin (50 μg/ml), chloramphenicol (20 μg/ml), and kanamycin (50 μg/ml) when appropriate. aTc (100 ng/ml) was supplemented when conditionally lethal KS310 and its derivatives were grown unless these cells were followed by the depletion of PE. $MgCl_2$ (50 mM) was supplemented when PE-deficient cells were grown. All cells were grown at 37°C unless indicated.

Construction of *E. coli* mutants

Strain KS310 was constructed as follows. The gene cassette that encodes the *tetR* gene under the control of the N25 promoter and the *pssA* gene under the control of $P_{LtetO-1}$, which is integrated into the *attP* site on the chromosome of AT210 (a *recA*$^+$ version of AT2033: Δ*pssA93*::*kan* Δ*lacY*::*Tn9 recA*$^-$ *srl*::*Tn10* $P_{LtetO-1}$-*pssA*) (*41*), was introduced into W3110 via P1 transduction. A Δ*pssA93*::*kan* mutation of AD90 (Δ*pssA93*::*kan*)/pDD72 (*pssA*$^+$) (*23*) was introduced into W3110/$P_{LtetO-1}$-*pssA* via P1 transduction, yielding KS310. BKT10 (W3110 Δ*clsA*), BKT16 (W3110 Δ*clsB* Δ*clsC*), and BKT12 (W3110 Δ*clsA* Δ*clsB* Δ*clsC*) were used as a host to construct KS510, KS610, and KS410, respectively.

Strain ADC90/pTac-ClsA (EE) was constructed as follows. A *clsA*::*Tn10* mutation of QC30-15 (*73*) was introduced into AD90/pDD72 (*23*) via P1 transduction, resulting in ADC90/pDD72. After transformation with pTac-ClsA (EE), the pDD72 plasmid was cured by growing at 42°C as shown previously (*23*).

Strain UE91 was constructed as follows: A Δ*clsA*::*kan*, Δ*clsB*::*kan*, or Δ*clsC*::*kan* gene was introduced into UE81 one by one via P1 transduction. The *kan* cassette in the intermediate strains was removed using plasmid pCP20, as described before (*74*, *75*).

Endogenous cysteine accessibility method

An overnight culture of *E. coli* cells was diluted to OD_{600} 0.05 in 200 ml of LB medium. After growing the cells until the mid-log phase (OD_{600} 0.6 to 0.8) at 37°C, cells were collected by centrifugation and then washed with buffer A [100 mM Hepes/KOH (pH 7.5), 80 mM NaCl, and 25 mM $MgCl_2$] and then resuspended in 2.5 ml of the same buffer. Cells were grown in LB or LB/0.5 M NaCl medium until the cell density reached OD_{600} 0.6 and then collected by centrifugation for osmotic up-shock or down-shock experiments. Collected cells were resuspended in 2.5 ml of buffer A containing 0.5 M NaCl for osmotic up-shock or in buffer A containing no NaCl for osmotic down-shock. The cell suspension was divided into three aliquots of 0.75 ml each. One aliquot was treated with 1 mM AMS for 60 min at 25°C to label cysteine residues exposed to the periplasmic side of the IM. To simultaneously label cysteine residues exposed to both sides of the IM, one aliquot was subjected to sonication for 1 min. After the sonication, the aliquot was treated with 1 mM AMS for 60 min at 25°C. The remaining aliquot was incubated without the addition of AMS. After labeling, the reactions were terminated by addition of 20 mM β-mercaptoethanol (β-ME). Both nontreated and AMS-treated aliquots without sonication were subjected to sonication. Unbroken cells were removed by centrifugation, and the membrane was collected by ultracentrifugation (88,000*g*) for 10 min at 4°C. The collected membrane fraction was resuspended in 100 μl of buffer A containing 20 mM β-ME. A 5- to 10-μl sample was subjected to SDS/PAGE and immunoblotting. The membrane fraction dissolved in the SDS-PAGE sample buffer was incubated at 37°C for 10 min before loading to the acrylamide gel. ClsA (EE) was detected using an anti–EE tag antibody after electroblotting. All ECAM analysis was performed at least twice.

TLC analysis of phospholipid extracts

E. coli cells were grown in LB with [^{32}P]PO_4 (1 μCi/ml) until the cell density reached OD_{600} 0.6 to 0.8. For lipid extraction, cells were collected by centrifugation and then resuspended in 0.2 ml of an acidic solution (0.5 M NaCl in 0.1 M HCl). Then, 0.6 ml of chloroform/methanol (1:2, v/v) was added and vortexed for 30 min. After that,

another 0.2 ml of a resuspension buffer was added with continued vortexing for another 10 min. The water and chloroform phases were separated by centrifugation (20,000*g* for 5 min), and the chloroform phase was collected. About 1000 to 2000 cpm of the phospholipid extract was applied to TLC plates. Individual phospholipids were separated either by solvent 1 [chloroform/methanol/acetic acid (60/25/8, v/v/v)] or by solvent 2 [chloroform/methanol/ammonia/water (65/37.5/3/1, v/v/v/v)]. Radiolabeled phospholipids were detected using a Typhoon FLA 9500 Phosphoimager and quantified by ImageQuant. All TLC analyses were performed at least twice.

EryA-EGFP binding assay

ISOv were prepared as described previously (*4*). Briefly, cells pellets were resuspended in 100 mM Hepes/KOH (pH 7.5) containing 25 mM $MgCl_2$. Total cell lysates were prepared by subjecting the cell suspensions to a single passage through a French press at 560 kg/cm^2 (8000 psi). Undisrupted cells and OM vesicles were removed from the lysate by centrifugation at 30,000*g* for 20 min. The ISOv were then collected by centrifugation at 200,000*g* for 1 hour and resuspended in 100 mM Hepes/KOH (pH 7.5) containing 250 mM sucrose and 5 mM $MgCl_2$ at a protein concentration of 5 to 10 mg/ml, and aliquots were stored at −80°C for subsequent use. Two hundred micrograms of the ISOv protein (final concentration of 1 mg/ml) was mixed with 50 nM purified EryA-EGFP and then incubated for 30 min at 37°C. ISOv were reisolated by ultracentrifugation (150,000*g*) for 20 min at 4°C. Isolated ISOv were resuspended in 100 μl of 100 mM Hepes/KOH (pH 7.5) followed by ultracentrifugation at the same speed. ISOv were resuspended in 100 μl of 100 mM Hepes/KOH (pH 7.5). The fluorescence intensity of EGFP bound to ISOv was measured using a Typhoon FLA 9500 and quantified by ImageQuant. For detection of EryA-EGFP by Western blotting, ISOv were resuspended in the SDS-PAGE sample buffer and subjected to SDS-PAGE and immunoblotting with antibodies against EGFP.

Statistical analysis

The results of quantitative experiments are shown as means for independent experiments performed multiple times as indicated. Values are means (± SD) from three experiments, where each determination was done in duplicate. Variation between duplicates was ±3%. The statistical significance of mean differences was assessed using the two-tailed Student's *t* test. Images represent three independent experiments.

Supplementary Materials

This PDF file includes:

Section S1
Figs. S1 to S16
Tables S1 to S3
References

REFERENCES AND NOTES

1. M. Bogdanov, The power and challenge of lipid (a)symmetry across the membrane and cell. *Emerg. Top. Life Sci.* **7**, 1–6 (2023).
2. M. Doktorova, J. L. Symons, I. Levental, Structural and functional consequences of reversible lipid asymmetry in living membranes. *Nat. Chem. Biol.* **16**, 1321–1330 (2020).
3. M. Bogdanov, Renovating a double fence with or without notifying the next door and across the street neighbors: Why the biogenic cytoplasmic membrane of Gram-negative bacteria display asymmetry? *Emerg. Top. Life Sci.* **7**, 137–150 (2023).
4. M. Bogdanov, K. Pyrshev, S. Yesylevskyy, S. Ryabichko, V. Boiko, P. Ivanchenko, R. Kiyamova, Z. Guan, C. Ramseyer, W. Dowhan, Phospholipid distribution in the cytoplasmic membrane of Gram-negative bacteria is highly asymmetric, dynamic, and cell shape-dependent. *Sci. Adv.* **6**, eaaz6333 (2020).
5. B. K. Tan, M. Bogdanov, J. Zhao, W. Dowhan, C. R. H. Raetz, Z. Guan, Discovery of a cardiolipin synthase utilizing phosphatidylethanolamine and phosphatidylglycerol as substrates. *Proc. Natl. Acad. Sci. U.S.A.* **109**, 16504–16509 (2012).
6. D. Guo, B. E. Tropp, A second *Escherichia coli* protein with CL synthase activity. *Biochim. Biophys. Acta* **1483**, 263–274 (2000).
7. A. Ohta, T. Obara, Y. Asami, I. Shibuya, Molecular cloning of the *cls* gene responsible for cardiolipin synthesis in *Escherichia coli* and phenotypic consequences of its amplification. *J. Bacteriol.* **163**, 506–514 (1985).
8. S. Nishijima, Y. Asami, N. Uetake, S. Yamagoe, A. Ohta, I. Shibuya, Disruption of the *Escherichia coli cls* gene responsible for cardiolipin synthesis. *J. Bacteriol.* **170**, 775–780 (1988).
9. V. W. Rowlett, V. K. P. S. Mallampalli, A. Karlstaedt, W. Dowhan, H. Taegtmeyer, W. Margolin, H. Vitrac, Impact of membrane phospholipid alterations in *Escherichia coli* on cellular function and bacterial stress adaptation. *J. Bacteriol.* **199**, e00849-16 (2017).
10. S. Ryabichko, V. d. M. Ferreira, H. Vitrac, R. Kiyamova, W. Dowhan, M. Bogdanov, Cardiolipin is required in vivo for the stability of bacterial translocon and optimal membrane protein translocation and insertion. *Sci. Rep.* **10**, 6296 (2020).
11. J. F. Nepper, Y. C. Lin, D. B. Weibel, Rcs phosphorelay activation in cardiolipin-deficient *Escherichia coli* reduces biofilm formation. *J. Bacteriol.* **201**, e00804-18 (2019).
12. M. V. Douglass, F. Cléon, M. S. Trent, Cardiolipin aids in lipopolysaccharide transport to the gram-negative outer membrane. *Proc. Natl. Acad. Sci. U.S.A.* **118**, e2018329118 (2021).
13. E. Mileykovskaya, I. Fishov, X. Fu, B. D. Corbin, W. Margolin, W. Dowhan, Effects of phospholipid composition on MinD-membrane interactions *in vitro* and *in vivo*. *J. Biol. Chem.* **278**, 22193–22198 (2003).
14. L. D. Renner, D. B. Weibel, MinD and MinE interact with anionic phospholipids and regulate division plane formation in *Escherichia coli*. *J. Biol. Chem.* **287**, 38835–38844 (2012).
15. T. Sakihara, N. Takiguchi, H. Uzawa, R. Serizawa, T. Kobayashi, Erylysin A inhibits cytokinesis in *Escherichia coli* by binding with cardiolipin. *J. Biochem.* **170**, 369–377 (2021).
16. Z. Zhou, K. A. White, A. Polissi, C. Georgopoulos, C. R. Raetz, Function of *Escherichia coli* MsbA, an essential ABC family transporter, in lipid A and phospholipid biosynthesis. *J. Biol. Chem.* **273**, 12466–12475 (1998).
17. C. M. Ernst, P. Staubitz, N. N. Mishra, S.-J. Yang, G. Hornig, H. Kalbacher, A. S. Bayer, D. Kraus, A. Peschel, The bacterial defensin resistance protein MprF consists of separable domains for lipid lysinylation and antimicrobial peptide repulsion. *PLOS Pathog.* **5**, e1000660 (2009).
18. D. Song, H. Jiao, Z. Liu, Phospholipid translocation captured in a bifunctional membrane protein MprF. *Nat. Commun.* **12**, 2927 (2021).
19. I. Shibuya, S. Yamagoe, C. Miyazaki, H. Matsuzaki, A. Ohta, Biosynthesis of novel acidic phospholipid analogs in *Escherichia coli*. *J. Bacteriol.* **161**, 473–477 (1985).
20. T. Romantsov, K. Gonzalez, N. Sahtout, D. E. Culham, C. Coumoundouros, J. Garner, C. H. Kerr, L. Chang, R. J. Turner, J. M. Wood, Cardiolipin synthase A colocalizes with cardiolipin and osmosensing transporter ProP at the poles of *Escherichia coli* cells. *Mol. Microbiol.* **107**, 623–638 (2018).
21. M. Bogdanov, W. Dowhan, "Functional roles of lipids in biological membranes" in *Biochemistry of Lipids, Lipoproteins and Membranes* (Elsevier Science, ed. 7, 2021).
22. A. G. Rietveld, V. V. Chupin, M. C. Koorengevel, H. L. Wienk, W. Dowhan, B. de Kruijff, Regulation of lipid polymorphism is essential for the viability of phosphatidylethanolamine-deficient *Escherichia coli* cells. *J. Biol. Chem.* **269**, 28670–28675 (1994).
23. A. DeChavigny, P. N. Heacock, W. Dowhan, Sequence and inactivation of the *pss* gene of *Escherichia coli*. Phosphatidylethanolamine may not be essential for cell viability. *J. Biol. Chem.* **266**, 5323–5332 (1991).
24. P. Gangola, B. P. Rosen, Maintenance of intracellular calcium in *Escherichia coli*. *J. Biol. Chem.* **262**, 12570–12574 (1987).
25. J. E. Lusk, E. P. Kennedy, Magneisum transport in *Escherichia coli*. *J. Biol. Chem.* **244**, 1653–1655 (1969).
26. M. Bogdanov, H. Vitrac, W. Dowhan, "Flip-flopping membrane proteins: How the charge balance rule governs dynamic membrane protein topology" in *Biogenesis of Fatty Acids, Lipids and Membranes* (Springer International Publishing, 2018), pp. 1–28.
27. S. Czolkoss, C. Fritz, G. Hölzl, M. Aktas, Two distinct cardiolipin synthases operate in *Agrobacterium tumefaciens*. *PLOS ONE* **11**, e0160373 (2016).
28. R. M. Rossi, L. Yum, H. Agaisse, S. M. Payne, Cardiolipin synthesis and outer membrane localizatfion are required for *Shigella flexneri* virulence. *mBio* **8**, e01199-17 (2017).
29. J. K. Chu, S. Zhu, C. M. Herrera, J. C. Henderson, J. Liu, M. S. Trent, T. R. Hoover, Loss of a cardiolipin synthase in *Helicobacter pylori* G27 blocks flagellum assembly. *J. Bacteriol.* **201**, e00372-19 (2019).
30. R. Lutz, H. Bujard, Independent and tight regulation of transcriptional units in *Escherichia coli* via the LacR/O, the TetR/O and AraC/I1-I2 regulatory elements. *Nucleic Acids Res.* **25**, 1203–1210 (1997).

31. I. Shibuya, C. Miyazaki, A. Ohta, Alteration of phospholipid composition by combined defects in phosphatidylserine and cardiolipin synthases and physiological consequences in *Escherichia coli*. *J. Bacteriol.* **161**, 1086–1092 (1985).
32. A. Nishibori, J. Kusaka, H. Hara, M. Umeda, K. Matsumoto, Phosphatidylethanolamine domains and localization of phospholipid synthases in *Bacillus subtilis* membranes. *J. Bacteriol.* **187**, 2163–2174 (2005).
33. M. Exterkate, N. A. W. de Kok, R. L. H. Andringa, N. H. J. Wolbert, A. J. Minnaard, A. J. M. Driessen, A promiscuous archaeal cardiolipin synthase enables construction of diverse natural and unnatural phospholipids. *J. Biol. Chem.* **296**, 100691 (2021).
34. B. R. Quigley, B. E. Tropp, *E. coli* cardiolipin synthase: Function of N-terminal conserved residues. *Biochim. Biophys. Acta* **1788**, 2107–2113 (2009).
35. G. von Heijne, Y. Gavel, Topogenic signals in integral membrane proteins. *Eur. J. Biochem.* **174**, 671–678 (1988).
36. G. von Heijne, Membrane-protein topology. *Nat. Rev. Mol. Cell Biol.* **7**, 909–918 (2006).
37. J. Jumper, R. Evans, A. Pritzel, T. Green, M. Figurnov, O. Ronneberger, K. Tunyasuvunakool, R. Bates, A. Žídek, A. Potapenko, A. Bridgland, C. Meyer, S. A. A. Kohl, A. J. Ballard, A. Cowie, B. Romera-Paredes, S. Nikolov, R. Jain, J. Adler, T. Back, S. Petersen, D. Reiman, E. Clancy, M. Zielinski, M. Steinegger, M. Pacholska, T. Berghammer, S. Bodenstein, D. Silver, O. Vinyals, A. W. Senior, K. Kavukcuoglu, P. Kohli, D. Hassabis, Highly accurate protein structure prediction with AlphaFold. *Nature* **596**, 583–589 (2021).
38. W. Dowhan, H. Vitrac, M. Bogdanov, Lipid-assisted membrane protein folding and topogenesis. *Protein J.* **38**, 274–288 (2019).
39. W. Dowhan, M. Bogdanov, Lipid-dependent membrane protein topogenesis. *Annu. Rev. Biochem.* **78**, 515–540 (2009).
40. M. Bogdanov, P. N. Heacock, W. Dowhan, A polytopic membrane protein displays a reversible topology dependent on membrane lipid composition. *EMBO J.* **21**, 2107–2116 (2002).
41. M. Bogdanov, J. Xie, P. Heacock, W. Dowhan, To flip or not to flip: Lipid-protein charge interactions are a determinant of final membrane protein topology. *J. Cell Biol.* **182**, 925–935 (2008).
42. X. Wang, M. Bogdanov, W. Dowhan, Topology of polytopic membrane protein subdomains is dictated by membrane phospholipid composition. *EMBO J.* **21**, 5673–5681 (2002).
43. H. Vitrac, M. Bogdanov, W. Dowhan, *In vitro* reconstitution of lipid-dependent dual topology and postassembly topological switching of a membrane protein. *Proc. Natl. Acad. Sci. U.S.A.* **110**, 9338–9343 (2013).
44. H. Vitrac, W. Dowhan, M. Bogdanov, Effects of mixed proximal and distal topogenic signals on the topological sensitivity of a membrane protein to the lipid environment. *Biochim. Biophys. Acta Biomembr.* **1859**, 1291–1300 (2017).
45. S. Hiraoka, K. Nukui, N. Uetake, A. Ohta, I. Shibuya, Amplification and substantial purification of cardiolipin synthase of *Escherichia coli*. *J. Biochem.* **110**, 443–449 (1991).
46. L. Ragolia, B. E. Tropp, The effects of phosphoglycerides on *Escherichia coli* cardiolipin synthase. *Biochim. Biophys. Acta* **1214**, 323–332 (1994).
47. A. Rath, M. Glibowicka, V. G. Nadeau, G. Chen, C. M. Deber, Detergent binding explains anomalous SDS-PAGE migration of membrane proteins. *Proc. Natl. Acad. Sci. U.S.A.* **106**, 1760–1765 (2009).
48. M. Bogdanov, W. Zhang, J. Xie, W. Dowhan, Transmembrane protein topology mapping by the substituted cysteine accessibility method (SCAM™): Application to lipid-specific membrane protein topogenesis. *Methods* **36**, 148–171 (2005).
49. M. Bogdanov, Mapping of membrane protein topology by Substituted Cysteine Accessibility Method (SCAM™). *Methods Mol. Biol.* **1615**, 105–128 (2017).
50. M. Bogdanov, Exploring uniform, dual, and dynamic topologies of membrane proteins by Substituted Cysteine Accessibility Method (SCAM™). *Methods Mol. Biol.* **2715**, 121–157 (2024).
51. W. Zhang, M. Bogdanov, J. Pi, A. J. Pittard, W. Dowhan, Reversible topological organization within a polytopic membrane protein is governed by a change in membrane phospholipid composition. *J. Biol. Chem.* **278**, 50128–50135 (2003).
52. A. Nichtl, J. Buchner, R. Jaenicke, R. Rudolph, T. Scheibel, Folding and association of β-galactosidase. *J. Mol. Biol.* **282**, 1083–1091 (1998).
53. M. Exterkate, "Sustainable membrane biosynthesis for synthetic minimal cells," thesis, University of Groningen, Groningen (2019).
54. J. K. Laws, R. E. Dalbey, Positive charges in the cytoplasmic domain of *Escherichia coli* leader peptidase prevent an apolar domain from functioning as a signal. *EMBO J.* **8**, 2095–2099 (1989).
55. C. Rutz, W. Rosenthal, R. Schülein, A single negatively charged residue affects the orientation of a membrane protein in the inner membrane of *Escherichia coli* only when it is located adjacent to a transmembrane domain. *J. Biol. Chem.* **274**, 33757–33763 (1999).
56. P. Li, J. Beckwith, H. Inouye, Alteration of the amino terminus of the mature sequence of a periplasmic protein can severely affect protein export in *Escherichia coli*. *Proc. Natl. Acad. Sci. U.S.A.* **85**, 7685–7689 (1988).
57. W. Zhang, H. A. Campbell, S. C. King, W. Dowhan, Phospholipids as determinants of membrane protein topology. Phosphatidylethanolamine is required for the proper topological organization of the γ-aminobutyric acid permease (GabP) of *Escherichia coli*. *J. Biol. Chem.* **280**, 26032–26038 (2005).
58. H. Andersson, G. von Heijne, A 30-residue-long "export initiation domain" adjacent to the signal sequence is critical for protein translocation across the inner membrane of *Escherichia coli*. *Proc. Natl. Acad. Sci. U.S.A.* **88**, 9751–9754 (1991).
59. Y. Tsatskis, J. Khambati, M. Dobson, M. Bogdanov, W. Dowhan, J. M. Wood, The osmotic activation of transporter ProP is tuned by both its C-terminal coiled-coil and osmotically induced changes in phospholipid composition. *J. Biol. Chem.* **280**, 41387–41394 (2005).
60. N. Levina, S. Tötemeyer, N. R. Stokes, P. Louis, M. A. Jones, I. R. Booth, Protection of *Escherichia coli* cells against extreme turgor by activation of MscS and MscL mechanosensitive channels: Identification of genes required for MscS activity. *EMBO J.* **18**, 1730–1737 (1999).
61. T. Kakuda, Y. Koide, A. Sakamoto, S. Takai, Characterization of two putative mechanosensitive channel proteins of *Campylobacter jejuni* involved in protection against osmotic downshock. *Vet. Microbiol.* **160**, 53–60 (2012).
62. D. R. Williamson, K. K. Dewan, T. Patel, C. M. Wastella, G. Ning, G. S. Kirimanjeswara, A single mechanosensitive channel protects Francisella tularensis subsp. holarctica from hypoosmotic shock and promotes survival in the aquatic environment. *Appl. Environ. Microbiol.* **84**, e02203-17 (2018).
63. R. Buda, Y. Liu, J. Yang, S. Hegde, K. Stevenson, F. Bai, T. Pilizota, Dynamics of *Escherichia coli*'s passive response to a sudden decrease in external osmolarity. *Proc. Natl. Acad. Sci. U.S.A.* **113**, E5838–E5846 (2016).
64. P. Ridone, Y. Nakayama, B. Martinac, A. R. Battle, Patch clamp characterization of the effect of cardiolipin on MscS of *E. coli*. *Eur. Biophys. J.* **44**, 567–576 (2015).
65. T. Romantsov, L. Stalker, D. E. Culham, J. M. Wood, Cardiolipin controls the osmotic stress response and the subcellular location of transporter ProP in *Escherichia coli*. *J. Biol. Chem.* **283**, 12314–12323 (2008).
66. E. Mileykovskaya, W. Dowhan, Visualization of phospholipid domains in *Escherichia coli* by using the cardiolipin-specific fluorescent dye 10-*N*-nonyl acridine orange. *J. Bacteriol.* **182**, 1172–1175 (2000).
67. C. Rathmann, A. S. Schlösser, J. Schiller, M. Bogdanov, T. Brüser, Tat transport in *Escherichia coli* requires zwitterionic phosphatidylethanolamine but no specific negatively charged phospholipid. *FEBS Lett.* **591**, 2848–2858 (2017).
68. I. J. Roney, D. Z. Rudner, The DedA superfamily member PetA is required for the transbilayer distribution of phosphatidylethanolamine in bacterial membranes. *Proc. Natl. Acad. Sci. U.S.A.* **120**, e2301979120 (2023).
69. H. Todor, N. Herrera, C. Gross, Three bacterial DedA subfamilies with distinct functions and phylogenetic distribution. *mBio* **14**, e0002823 (2023).
70. L. Wang, P. Bütikofer, Lactose permease scrambles phospholipids. *Biology* **12**, 1367 (2023).
71. D. Li, C. Rocha-Roa, M. A. Schilling, K. M. Reinisch, S. Vanni, Lipid scrambling is a general feature of protein insertases. *Proc. Natl. Acad. Sci. U.S.A.* **121**, e2319476121 (2024).
72. R. Moser, M. Aktas, C. Fritz, F. Narberhaus, Discovery of a bifunctional cardiolipin/phosphatidylethanolamine synthase in bacteria. *Mol. Microbiol.* **92**, 959–972 (2014).
73. B. E. Tropp, L. Ragolia, W. Xia, W. Dowhan, R. Milkman, K. E. Rudd, R. Ivanisević, D. J. Savić, Identity of the *Escherichia coli cls* and *nov* genes. *J. Bacteriol.* **177**, 5155–5157 (1995).
74. P. P. Cherepanov, W. Wackernagel, Gene disruption in *Escherichia coli*: Tc^R and Km^R cassettes with the option of Flp-catalyzed excision of the antibiotic-resistance determinant. *Gene* **158**, 9–14 (1995).
75. K. A. Datsenko, B. L. Wanner, One-step inactivation of chromosomal genes in *Escherichia coli* K-12 using PCR products. *Proc. Natl. Acad. Sci. U.S.A.* **97**, 6640–6645 (2000).
76. B. J. Bachmann, Pedigrees of some mutant strains of *Escherichia coli* K-12. *Bacteriol. Rev.* **36**, 525–557 (1972).
77. L. M. Guzman, D. Belin, M. J. Carson, J. Beckwith, Tight regulation, modulation, and high-level expression by vectors containing the arabinose P_{BAD} promoter. *J. Bacteriol.* **177**, 4121–4130 (1995).
78. T. Shibui, M. Uchida, Y. Teranishi, A new hybrid promoter and its expression vector in *Escherichia coli*. *Agric. Biol. Chem.* **52**, 983–988 (1988).

Acknowledgments: We would like to acknowledge T. Kobayashi (CNRS and Université de Strasbourg, France) and S. Sukharev (University of Maryland, College Park, Maryland) for EryA-EGFP and the MJF465 strain, respectively, and fruitful discussions. **Funding:** This work was supported by the NATO Science for Peace and Security Programme SPS 985291 (to M.B.), National Institutes of General Medical Sciences Grant R01GM121493-6 to M.B. and W.D. K.S. is a recipient of a scholarship from the Japan Society for the Promotion of Science and the Osamu Hayaishi Memorial Scholarship for Study Abroad under M.B.'s supervision. **Author contributions:** Each author's contributions to this paper are listed below. Writing—original draft: K.S. and M.B. Conceptualization: K.S. and M.B. Investigation: K.S. and M.B. Writing—

review and editing: K.S., M.B., and W.D. Methodology: K.S. and M.B. Resources: K.S. and M.B. Funding acquisition: K.S., M.B., and W.D. Data curation: K.S. and M.B. Validation: K.S. and M.B. Supervision: K.S. and M.B. Formal analysis: K.S. and M.B. Project administration: K.S. and M.B. Visualization: K.S. and M.B. All authors reviewed the results and approved the final version of the manuscript. **Competing interests:** The authors declare that they have no competing interests. **Data and materials availability:** All data needed to evaluate the conclusions in the paper are present in the paper and/or the Supplementary Materials. The bacterial strains and plasmids can be provided by M.B. pending scientific review and a completed material transfer agreement. Requests for the bacterial strains and plasmids should be submitted to M.B.

Submitted 27 July 2024
Accepted 2 December 2024
Published 3 January 2025
10.1126/sciadv.ads0244